Rifaximin prophylaxis causes resistance to the last-resort antibiotic daptomycin

A.M. Turner[1], L. Li[1], I.R. Monk[1], J.Y.H. Lee[1,2], D.J. Ingle[1], S. Portelli[3,4], N.L. Sherry[1,5,6], N. Isles[1], T. Seemann[1,5,7], L.K. Sharkey[1], C.J. Walsh[1], G.E. Reid[8,9,10], S. Nie[11], B.A. Eijkelkamp[12], N.E. Holmes[6,13], B. Collis[6], S. Vogrin[6,14], A. Hiergeist[15], D. Weber[16], A. Gessner[15], E. Holler[14], D.B. Ascher[3,4], S. Duchene[1], N.E. Scott[1], T.P. Stinear[1,7], J.C. Kwong[1,6], C.L. Gorrie[1,5,7]*, B.P. Howden[1,5,6,7]*† and G.P. Carter[1]*†

[1]Department of Microbiology and Immunology, The University of Melbourne at The Peter Doherty Institute for Infection and Immunity, Melbourne, VIC, Australia.

[2]Department of Infectious Diseases, Monash Health, Clayton, VIC, Australia.

[3]Computational Biology and Clinical Informatics, Baker Heart and Diabetes Institute, Melbourne, Victoria, Australia.

[4]SCMB, The University of Queensland, Saint Lucia Campus, Saint Lucia, Queensland, Australia.

[5]Microbiological Diagnostic Unit Public Health Laboratory, Department of Microbiology and Immunology, The University of Melbourne at The Peter Doherty Institute for Infection and Immunity, Melbourne, VIC, Australia.

[6]Department of Infectious Diseases & Immunology, Austin Health, Melbourne, VIC, Australia.

[7]Centre for Pathogen Genomics, The University of Melbourne, Melbourne, VIC, Australia.

[8]School of Chemistry, The University of Melbourne, Melbourne, VIC, Australia.

[9]Department of Biochemistry and Pharmacology, The University of Melbourne, Melbourne, VIC, Australia.

[10]Bio21 Molecular Science and Biotechnology Institute, The University of Melbourne, Melbourne, VIC, Australia.

[11]Melbourne Mass Spectrometry and Proteomics Facility, Bio21 Molecular Science and Biotechnology Institute, The University of Melbourne, Melbourne, VIC, Australia.

25 [12]Molecular Sciences and Technology, College of Science and Engineering, Flinders University,
26 Adelaide, SA, Australia.
27 [13]Department of Infectious Diseases, The University of Melbourne at The Peter Doherty
28 Institute for Infection and Immunity, Melbourne, VIC, Australia.
29 [14]Department of Medicine, The University of Melbourne, Melbourne, VIC, Australia.
30 [15]Institute of Clinical Microbiology and Hygiene, University Medical Center, Regensburg,
31 Germany.
32 [16]Department of Internal Medicine III, Hematology and Medical Oncology, University Medical
33 Center, Regensburg, Germany.
34 *These authors supervised this work equally.
35 †**Corresponding authors:** glen.carter@unimelb.edu.au, bhowden@unimelb.edu.au
36

37 **Abstract**

38 Multidrug-resistant bacterial pathogens like vancomycin-resistant *Enterococcus faecium*
39 (VREfm) are a critical threat to human health. Daptomycin is a last-resort antibiotic for VREfm
40 infections with a novel mode-of-action, but for which resistance has surprisingly been widely
41 reported but unexplained. Here we show that rifaximin, an unrelated antibiotic used
42 prophylactically to prevent hepatic encephalopathy in liver disease patients, causes cross-
43 resistance to daptomycin in VREfm. Amino acid changes arising within the bacterial RNA
44 polymerase in response to rifaximin exposure cause upregulation of a previously
45 uncharacterised operon (*prdRAB*) that leads to cell membrane remodelling and cross-
46 resistance to daptomycin through reduced binding of the antibiotic. Alarmingly, VREfm with
47 these mutations are spread globally, making this a major mechanism of resistance. Rifaximin
48 has been considered 'low-risk' for antibiotic resistance development. Our study shows this

assumption is flawed and widespread rifaximin use, particularly in patients with liver cirrhosis, may be compromising the clinical use of daptomycin, a major last-resort intervention for multidrug-resistant pathogens. These findings demonstrate how unanticipated antibiotic cross-resistance can undermine global strategies designed to preserve the clinical use of critical antibiotics.

Main

Antimicrobial resistance (AMR) is one of the greatest public health threats, with 1.27 million deaths being directly attributable to bacterial AMR in 2019[1]. The magnitude of this threat is therefore similar to that of malaria (558,000 global deaths in 2019)[2], HIV (690,000 deaths in 2019)[3], and diabetes mellitus (1.5 million deaths in 2019)[4]. Infections caused by multidrug- and extensively-drug resistant pathogens are of particular clinical concern since they are associated with frequent treatment failure and high-rates of morbidity and mortality. The preservation of last-resort antibiotics that can be used to treat these formidable pathogens is of critical importance.

Enterococcus faecium is one such formidable pathogen. It is a commensal of the human gastrointestinal tract that has emerged as a major cause of nosocomial infections[5]. The intrinsic antibiotic resistance of hospital-associated clones coupled with their ability to rapidly acquire additional antibiotic resistance genes makes *E. faecium* infections increasingly difficult to treat[6]. In particular, strains resistant to vancomycin, the first-line antibiotic for invasive infections, have emerged and disseminated globally due to the acquisition of transferable *van* resistance genes[7]. Consequently, *E. faecium*, which is one of the ESKAPE[8] pathogens, has been recognised by the World Health Organization (WHO) as a 'high priority' bacterial pathogen[9].

73

74 The lipopeptide daptomycin is a WHO designated last-resort antibiotic that is used 'off-label'
75 to treat severe vancomycin-resistant *E. faecium* (VREfm) infections[10]. The increasing reports
76 of daptomycin-resistant VREfm are of great clinical concern. Daptomycin resistance in clinical
77 VREfm has been associated with the presence of specific amino acid changes in the regulatory
78 systems LiaFSR/LiaXYZ and cardiolipin synthase Cls[11–13]. However, many daptomycin-resistant
79 VREfm contain wild-type (WT) *liaFSR/liaXYZ* and *cls* alleles, indicating other unknown
80 molecular pathways are involved[12,14,15].

81

82 In Australia, high rates (15%) of daptomycin-resistant VREfm were recently reported[16], but the
83 data were not epidemiologically robust and the specific genetic determinants leading to
84 resistance were not defined using molecular techniques. Accordingly, we undertook a
85 combined genomic and phenotypic analysis to investigate the daptomycin resistance
86 mechanisms in VREfm. Here we show that daptomycin resistance is linked with the presence
87 of specific mutations within the *rpoB* gene, with resistance emerging *de novo* in *E. faecium*
88 following exposure to rifaximin, a commonly prescribed antibiotic used prophylactically to
89 prevent hepatic encephalopathy in liver disease patients[17]. The emergence of these
90 daptomycin-associated *rpoB* mutations leads to transcriptional reprogramming in VREfm and
91 daptomycin resistance via a mechanism that is independent of previously described systems,
92 such as the *lia* operons or *cls.* Instead, the daptomycin-associated *rpoB* mutations cause
93 upregulation of a previously uncharacterised genetic locus that results in cell membrane
94 remodelling, which ultimately increases the cell surface charge and reduces daptomycin
95 binding. Our work has uncovered a major new mechanism of daptomycin resistance in VREfm

96 and identified rifaximin, an antibiotic considered to be low-risk for the emergence of bacterial
97 AMR[18], as an important driver of last-resort antibiotic resistance.
98
99 **Results**
100 **Daptomycin resistance in Australian VREfm is polygenic and does not correlate with known**
101 **resistance determinants.**
102 Daptomycin susceptibility testing was performed on VREfm isolated during two unbiased
103 state-wide 'snapshot' studies undertaken for month-long periods in 2015 (n=294) and 2018
104 (n=423) in Victoria, Australia. The proportion of daptomycin-resistant isolates was 16.6%
105 (n=49) in 2015 and 15.3% (n=65) in 2018. Given the high-rate of resistance observed, we
106 expanded the study to include VREfm isolated in 2017 (n=108) and 2018 (n=173) as part of
107 the 'Controlling Superbugs' study[19,20], with 28.4% (n=80) of these isolates being resistant to
108 daptomycin. Overall, we observed 194 (19.4%) daptomycin-resistant VREfm isolates,
109 indicating a very high prevalence of daptomycin resistance in Victoria, Australia.
110
111 To investigate the relationship between daptomycin-resistant and daptomycin-susceptible
112 VREfm, a maximum-likelihood phylogeny was inferred from an alignment of 6,574 core
113 genome single nucleotide polymorphisms (SNPs) (n=1000; 998 study isolates and two
114 controls) (Supplementary Figure 1). *In silico* multi-locus sequence typing identified 36
115 sequence types (STs) within the 1000 isolates; 30 of these STs included at least one of the
116 daptomycin-resistant VREfm. Daptomycin resistance was polyphyletic, with several distinct
117 clades. The largest clade (ST203) of daptomycin-resistant strains, accounted for 41.2% of
118 resistant isolates (n=80 of 194) and consisted of a predominant clone during our sampling
119 timeframe (2015 to 2018), suggestive of an expanding daptomycin-resistant lineage. The

120 other predominant STs (ST80, ST796, ST1421, and ST1424) consisted of several groups of
121 resistant isolates that did not cluster based on tree structure. The presence of daptomycin-
122 resistant isolates in distinct genetic backgrounds suggested daptomycin resistance has arisen
123 independently in VREfm on multiple occasions.
124
125 We next sought to determine the genetic determinants leading to daptomycin resistance in
126 Australian VREfm. We systematically screened VREfm genomes for mutations in the regulatory
127 genes *liaFSR*, *liaXYZ*, *yycFG* (*walKR*), cardiolipin synthase *(cls)*, and the division site
128 tropomyosin locus (*divIVA*), all previously linked to daptomycin resistance[10,11,21].
129 Unexpectedly, there were no significant associations with daptomycin resistance and
130 mutations in these loci (Supplementary Table 1).
131
132 **The S491F substitution in RpoB is a novel mediator of daptomycin resistance in VREfm.**
133 To identify the loci linked with daptomycin resistance, we performed a genome-wide
134 association study (GWAS) with 1000 *E. faecium* isolates (Figure 1A). This analysis identified
135 142 mutations (in 73 genes) significantly ($P<1x10^{-10}$) associated with daptomycin resistance
136 (as a binary variable with a breakpoint of 8 mg L^{-1}). The top five significant amino acid
137 substitutions were (i) I274S in an uncharacterised ABC efflux protein ($P=7.44x10^{-15}$), (ii) G71S
138 in an uncharacterised permease protein ($P=7.77x10^{-14}$), (iii) V288L in a mannitol
139 dehydrogenase protein ($P=6.08x10^{-12}$), (iv) S491F in RpoB, which is the RNA polymerase ß
140 subunit ($P=1.57x10^{-13}$), and (v) T634K in RpoC, which is the RNA polymerase ß' subunit
141 ($P=4.40x10^{-11}$).
142

143 To test the contribution of these amino acid substitutions on daptomycin resistance we
144 engineered each mutation into a clinical daptomycin-susceptible strain of VREfm (ST796).
145 Introduction of the I274S substitution in the ABC efflux protein, G71S substitution in the
146 permease protein, V288L substitution in the mannitol dehydrogenase protein, or T634K
147 substitution within RpoC had no impact on daptomycin susceptibility. However, introduction
148 of the S491F substitution within RpoB resulted in a daptomycin-resistant phenotype (4-fold
149 increase in daptomycin MIC, from 2 mg L^{-1} to 8 mg L^{-1}). Interestingly, every clinical strain
150 harbouring the RpoB S491F substitution (n=105, spanning different *E. faecium* genotypes) also
151 contained the RpoC T634K substitution (n=105), with no strains containing the RpoC T634K in
152 isolation. Introduction of the RpoC T634K substitution into the RpoB S491F mutant
153 background did not affect daptomycin susceptibility (MIC still 8 mg L^{-1}), suggesting this
154 mutation does not play a direct role in the daptomycin resistance phenotype and instead may
155 be compensatory for negative fitness effects associated with the RpoB S491F substitution. In
156 a competition assay (WT versus RpoB S491F or WT versus RpoB S491F/RpoC T634K), the RpoB
157 S491F substitution posed a substantial fitness cost, with a significant (P<0.0001) shift to the
158 WT population (Supplementary Figure 2). However, in the double RpoB S491F/RpoC T634K
159 mutant the population dynamics remained stable, with no significant differences compared
160 to inoculation observed (Supplementary Figure 2). These data suggest the RpoC T634K
161 substitution is compensatory for the negative fitness effects of RpoB S491F, a hypothesis
162 consistent with studies in *Mycobacterium tuberculosis*[22] and *Escherichia coli*[23].
163
164 **Different substitutions within the rifampicin resistance determining region of RpoB result in**
165 **daptomycin resistance in VREfm.**

166 We next assessed if other RpoB substitutions were associated with daptomycin resistance
167 (Figure 1B). We observed resistance in 81.3% of VREfm strains (n=16) with a G482D
168 substitution and 83.3% of VREfm strains (n=12) with a H486Y substitution. Isolates harbouring
169 these mutations were spread across the phylogenetic tree, indicative of multiple independent
170 acquisitions (Figure 1C). No putative compensatory mutations in the RNA polymerase genes
171 were identified. Clonal expansion was also observed for a dominant, daptomycin-resistant
172 clone (ST203) containing the S491F substitution. Daptomycin-resistant isolates from this
173 ST203 lineage were identified across 10 geographically distinct hospital networks, indicating
174 they were not part of a singular hospital outbreak (Supplementary Figure 3).
175
176 The G482D, H486Y, and S491F substitutions were located within the predicted rifampicin-
177 resistance determining region (RRDR) of RpoB (spanning amino acids 467 to 493). Rifampicin
178 susceptibility testing (rifampicin being a marker of rifamycin resistance[24]) confirmed all
179 isolates had high-level rifampicin resistance (n=169, median MIC 256 mg L^{-1}), while control
180 isolates containing the WT RRDR displayed a median MIC of 8 mg L^{-1} (n=169, Supplementary
181 Figure 4).
182
183 To test if the G482D and H486Y substitutions in RpoB also led to rifamycin and daptomycin
184 resistance we engineered isogenic mutants with these substitutions in our rifamycin-
185 susceptible, daptomycin-susceptible, clinical strain of VREfm (ST796). Introduction of the
186 G482D, H486Y, or S491F RpoB substitutions resulted in a 7-fold decrease in rifampicin
187 susceptibility compared to the WT strain, leading to high-level rifampicin resistance (>512 mg
188 L^{-1}) (Figure 1D). The introduction of the G482D or H486Y RpoB substitutions also resulted in a
189 daptomycin-resistant phenotype (4-fold increase in daptomycin MIC, from 2 mg L^{-1} to 8 mg L^{-}

190 ^{1}) (Figure 1E). Reverse allelic exchange with the WT *rpoB* allele resulted in susceptibility to
191 rifampicin (MIC of 4 mg L^{-1}) and daptomycin (MIC of 2 mg L^{-1}), confirming that G482D, H486Y,
192 and S491F caused rifamycin resistance and daptomycin cross-resistance.
193
194 **The G482D, H486Y, and S491F RpoB substitutions are common in international VREfm**
195 **strains.**
196 To determine if the RpoB substitutions associated with daptomycin resistance observed in
197 Australian VREfm were representative of other *E. faecium* globally, we analysed publicly
198 available VREfm sequence data (n=3,476 international and n=1,000 Australian) (Figure 2A).
199 The majority (n=3,378) of these VREfm were healthcare-associated, with 98 isolates from
200 animal origin. Of all the isolates analysed, 630 (14.1%) carried an amino acid substitution in
201 the RRDR of RpoB, with the S491F substitution being the most common, present in 77.9%
202 (n=461) of isolates with a RRDR RpoB substitution (Figure 2B). The S491F substitution was
203 identified in isolates from 20 countries and across 21 different STs (Figure 2B and
204 Supplementary Figure 5A). Importantly, five VREfm (from three genetic backgrounds and four
205 countries) harbouring the S491F substitution also contained *cfr(B)* (n=4) or *poxtA* (n=1)
206 linezolid resistance genes, suggesting near pan-resistant strains of VREfm have emerged. The
207 G482D and H486Y substitutions were also commonly identified, found in 6.8% (n=43) and
208 11.6% (n=73) of strains with the RpoB substitution, respectively. The G482D and H486Y
209 substitutions were also observed globally (7 and 10 countries, respectively) and across
210 different STs (9 and 22, respectively) (Figure 2B and Supplementary Figure 5A). These data
211 indicated the RpoB substitutions conferring resistance to rifamycins and cross-resistance to
212 daptomycin are globally prevalent. We also observed a significant association between RRDR
213 RpoB substitutions and healthcare-associated VREfm (P<0.001; Fisher's exact test)

214 (Supplementary Figure 5B)[25], suggesting the identified RpoB substitutions are enriched within
215 the healthcare setting.
216
217 **Phylodynamics show the S491F RpoB substitution emerged within the VREfm population in**
218 **the same period as the clinical approval of rifaximin.**
219 We used phylodynamic analyses to estimate the emergence date of VREfm harbouring the
220 S491F substitution globally. Within the genomes of Australian VREfm isolates, we observed
221 the expansion of a dominant ST203 clone from 2015 to 2018 that carried the S491F
222 substitution (Figure 1C). Since this clone comprised VREfm carrying the *vanA* resistance
223 operon, we genome sequenced all historical *vanA*-VREfm from our public health laboratory
224 (n=229), which consisted of every *vanA*-VREfm isolate collected from 2003 to 2014, to
225 increase the potential to detect a molecular clock signal. Using comparative genomics, we
226 contextualised all Australian isolates (n=1,229) with the international data (n=3,476) and
227 identified three distinct clusters containing the RpoB S491F substitution (Figure 2C). The same
228 ST203 clone formed the largest cluster (Cluster 1; n=219 taxa), consisting of isolates from
229 Australia and United Kingdom. Cluster 2 (n=85 taxa) consisted of ST80 and ST78 isolates from
230 Australia, Europe, South America, the United Kingdom, and the United States while Cluster 3
231 (n=68 taxa) consisted of ST80 isolates from Australia, Europe, and the United Kingdom.
232
233 To model the evolutionary trajectories of these clusters, we used core-genome SNP diversity
234 and year of isolation (Figure 2D and Supplementary Figure 6). The substitution rate (the
235 number of expected nucleotide substitutions per site per year) was consistent with other
236 estimates for healthcare-associated VREfm[25–28] (Figure 2D). The year of emergence for the
237 most recent common ancestor (MRCA) of each cluster with S491F was around 2006 (Figure

238 2D), a time period that coincides with the first clinical use of rifaximin. Since rifampicin was
239 approved for clinical use in the United States in 1971[29], several decades before the estimated
240 emergence of the S491F-containing VREfm strains, we considered this rifamycin unlikely to
241 have played a major role in the spread of resistance. Analysis of the three maximum clade
242 credibility (MCC) trees (Figure 2D) indicated each *E. faecium* lineage has continued to expand
243 since its emergence, consistent with the growing use of rifaximin globally, in particular since
244 2010 when it was approved for the prevention of hepatic encephalopathy[17] (Figure 2D-E). It
245 is also noteworthy that in all three VREfm clusters, the S491F substitution has been stably
246 maintained after its acquisition, suggestive of on-going selective pressure acting on the
247 bacterial population, as *rpoB* mutations usually carry a fitness cost (Supplementary Figure 7A-
248 C)[22]. These data show the S491F substitution emerged within the VREfm population on at least
249 three occasions since the early 2000s, with the predicted dates of emergence closely
250 correlated with the clinical introduction of rifaximin.
251
252 **Patients receiving rifaximin are more likely to carry VREfm with daptomycin resistance RpoB**
253 **substitutions than patients that have not received rifaximin.**
254 Rifaximin is a non-absorbable oral agent with direct antimicrobial activity in the
255 gastrointestinal tract, predominately prescribed to prevent recurrent hepatic encephalopathy
256 in patients with liver cirrhosis[17,30]. This patient cohort is high-risk for VREfm gastrointestinal
257 colonisation[31]. Since the Bayesian phylodynamic analyses highlighted a correlation between
258 the S491F RpoB substitution in VREfm and use of rifaximin, we hypothesised rifaximin use in
259 VREfm colonised patients may be associated with the presence of substitutions in RpoB and,
260 therefore, daptomycin resistance. To test this hypothesis, we assessed the association
261 between rifaximin exposure and daptomycin-resistant VREfm in a retrospective patient cohort

262 at a quaternary referral healthcare centre in Melbourne, Australia. The *E. faecium* isolates
263 from patients with current or prior rifaximin exposure – "rifaximin" group – and without prior
264 exposure ("control" group) were assessed a) genomically for the RpoB amino acid
265 substitutions (G482D, H486Y, and S491F) that result in daptomycin resistance and b)
266 phenotypically for daptomycin resistance, by study investigators blinded to patient details and
267 the exposure groups. The VREfm isolates were phylogenetically distributed and both rifaximin
268 and control group isolates were representative of the *E. faecium* strains identified in the state-
269 wide snapshot survey (Figure 3A)[32]. Isolates that were genomically clustered and likely to
270 represent patient-to-patient transmission were excluded from the analysis (see Methods).
271 Genetically distinct VREfm from 212 individual patients collected between 2014-2022 were
272 included in the analysis: 96 in the "rifaximin" exposed group and 116 in the unexposed
273 "control" group. Overall patient demographics of the cohort were balanced between the two
274 groups with the exceptions of age ($P<0.001$) and overall Charlson Comorbidity Index score
275 ($P<0.001$), which was driven by a significantly greater proportion of patients with chronic liver
276 disease in the rifaximin group ($P<0.001$) (Supplementary Table 2). As expected, there was also
277 significantly greater recent exposure to rifaximin (within the last 90 days prior to VREfm
278 sample collection) in the rifaximin group ($P<0.001$). Notably, only a single patient in the study
279 had received recent daptomycin.
280
281 Among the VREfm obtained from the entire (n=212) cohort, recent exposure to rifaximin was
282 significantly associated with the presence of RpoB substitutions ($P<0.001$), including
283 substitutions associated with daptomycin resistance (either G482D, H486Y, or S491F;
284 $P<0.001$), and was significantly associated with carriage of daptomycin-resistant VREfm
285 ($P<0.001$) (Figure 3B, Supplementary Table 3). More importantly, after adjusting for potential

286 confounders, recent rifaximin exposure remained an independent predictor of these
287 daptomycin resistance RpoB substitutions (OR 8.69; 95% CI 2.95-30.84; *P*<0.001) and
288 daptomycin-resistant VREfm (OR 6.47; 95% CI 2.34-20.80; *P*<0.001) among the overall cohort
289 of patients (Supplementary Table 4A-B). Given almost all patients who received rifaximin had
290 underlying chronic liver disease (with hepatic encephalopathy being the predominant
291 indication for rifaximin prescribing in Australia), we assessed the association between
292 rifaximin and daptomycin resistance first within the subgroup of patients with liver disease
293 (Supplementary Tables 5A-C), and then second, in an independent cohort of patients without
294 liver disease from the University Medical Center, Regensburg, Germany. These patients were
295 undergoing haematopoietic stem cell transplantation (HSCT), where rifaximin is used for
296 antimicrobial prophylaxis (Supplementary Tables 6A-C). The significant association between
297 rifaximin exposure and daptomycin resistance RpoB substitutions was again identified in both
298 patient groups – a) patients with chronic liver disease (*P*=0.001) and b) HSCT patients without
299 liver disease (*P*<0.001) (Supplementary Figure 10 and Supplementary Tables 5C and 6C).
300 Among the patients with liver disease colonised with VREfm, recent rifaximin was an
301 independent predictor of daptomycin-resistant VREfm (OR 4.37; 95% CI 1.70-12.84; *P*=0.004).
302 We conducted several other sensitivity analyses to verify the robustness of these associations
303 and assess for other confounders, including a subgroup analysis that excluded patients who
304 received rifaximin from the analysis (Supplementary Table 7), but these did not identify any
305 other associations between daptomycin resistance and underlying disease or antibiotic
306 exposure.
307
308 There were six patients from the "control" group with daptomycin-resistant VREfm – three
309 (50%) of these had isolates with no mutations in *rpoB*, suggesting an alternate mechanism for

310 resistance, while the remaining three patients had previously been admitted to the liver ward
311 for inpatient care, suggesting they may have acquired daptomycin-resistant VREfm through
312 healthcare-associated transmission.
313
314 While only one representative VREfm isolate from each patient was included in the above
315 analysis, the *de novo* emergence of daptomycin-resistant VREfm carrying the G482D RpoB
316 substitution was observed in one patient from whom multiple isolates were collected during
317 rifaximin therapy, consistent with rifaximin exposure driving the *de novo* emergence of
318 daptomycin-resistant VREfm.
319
320 Therefore, in agreement with our laboratory observations, these clinical data confirm a strong
321 clinical association between recent rifaximin exposure and *rpoB* substitutions linked to
322 daptomycin resistance among patients colonised with VREfm, suggesting exposure to
323 rifaximin could drive daptomycin-resistant VREfm.
324
325 **Rifaximin exposure leads to daptomycin-resistant VREfm in a murine model of**
326 **gastrointestinal colonisation.**
327 We next used a mouse VREfm gastrointestinal colonisation model to understand if rifaximin
328 exposure caused *de novo* emergence of *rpoB* mutations that confer cross-resistance to
329 daptomycin. Mice were colonised with a daptomycin-susceptible (MIC 2 mg L^{-1}) clinical VREfm
330 isolate (Aus0233) containing a WT *rpoB* allele before being administered a human-equivalent
331 dose of either rifaximin, rifampicin, daptomycin, or vehicle (Figure 4A and Supplementary
332 Figure 9). Rifampicin was chosen as a comparison since it is a rifamycin used in clinical practice.
333 After 7 days of rifamycin treatment, we observed rifamycin-resistant VREfm in significantly

334 more mice receiving rifampicin (80% of mice) or rifaximin (90% of mice) than in mice that
335 received daptomycin (0% of mice) (P<0.0001 and P<0.0001; unpaired t-test) or vehicle (0% of
336 mice) (P<0.0001 and P<0.0001; unpaired t-test) (Figure 4B).
337
338 For each mouse, we then determined the percentage of individual VREfm isolates that were
339 rifamycin-resistant or daptomycin-resistant. There were significantly more rifamycin-resistant
340 VREfm isolated from mice receiving rifaximin or rifampicin than mice receiving the vehicle
341 control (P<0.0001 and P<0.0001; unpaired t-test) or daptomycin (P<0.001 and P<0.001;
342 unpaired t-test) (Figure 4D). Similarly, there was significantly more daptomycin-resistant
343 VREfm in mice receiving rifaximin or rifampicin than vehicle control (P<0.05 and P<0.05;
344 unpaired t-test) or daptomycin (P<0.05 and P<0.05; unpaired t-test) (Figure 4E). We estimated
345 that daptomycin-resistant VREfm accounted for between 0-41% of the gastrointestinal VREfm
346 population in mice given rifaximin and 0-36% in mice given rifampicin, demonstrating
347 conclusively that rifamycin administration drives the emergence of VREfm with resistance to
348 rifamycins and cross-resistance to daptomycin. Notably, no daptomycin-resistant VREfm were
349 isolated from mice receiving daptomycin, in agreement with prior research[35].
350
351 We then performed WGS on 150 randomly selected VREfm isolates from each group (rifaximin
352 or rifampicin, n=300 total) to identify all mutations present in the rifamycin-resistant isolates.
353 This collection consisted of 100 rifaximin or rifampicin-resistant isolates taken following the
354 last day of treatment and 50 isolates from each group collected prior to rifamycin
355 administration. No substitutions in RpoB were identified in any *E. faecium* isolate taken prior
356 to rifaximin or rifampicin exposure. However, after exposure to either rifaximin or rifampicin,
357 VREfm carrying mutations within *rpoB* were commonly identified. The S491F substitution was

358 most prevalent (n=53 [rifaximin] and n=63 [rifampicin]), with all isolates carrying this
359 substitution being daptomycin-resistant (Figure 4F). The H486Y substitution was identified at
360 a reduced frequency compared to the S491F, (n=12 [rifaximin] and n=28 [rifampicin],
361 respectively), with all isolates again being daptomycin-resistant. The G482D substitution was
362 the third most commonly identified RpoB substitution (n=15 [rifaximin] and n=6 [rifampicin],
363 respectively), with 19 isolates carrying this substitution being daptomycin-resistant. Other
364 RpoB substitutions in addition to S491F, H486Y, and G482D were also identified. These
365 substitutions included V135F, L471V, Q473L, and H486R, however all VREfm isolates carrying
366 these substitutions were daptomycin-susceptible. Importantly, the proportions of each RpoB
367 substitution observed in VREfm collected from the gastrointestinal tract of mice administered
368 either rifaximin or rifampicin, closely matched the proportions of each mutation observed in
369 our collection of human clinical VREfm isolates, with the S491F substitution most commonly
370 identified, followed by H486Y, and then G482D. These observations in our mouse model
371 strongly suggest that exposure to rifaximin is driving the *de novo* emergence of daptomycin
372 resistance in colonising strains of *E. faecium* in humans.
373
374 **VREfm with daptomycin-resistant RpoB substitutions have changes in the cell membrane**
375 **lipid profile and increased expression of the *prdRAB* regulon.**
376 To understand how amino acid substitutions in the ß subunit of the bacterial RNA polymerase
377 (RpoB) cause resistance to daptomycin, a cell membrane active antibiotic, we utilised a multi-
378 omics approach. We started by analysing the lipidomes of the three isogenic daptomycin-
379 resistant RpoB mutants (G482D, H486Y, or S491F) compared to WT VREfm. We additionally
380 included an isogenic RpoB mutant that did not confer resistance to daptomycin (Q473L;
381 daptomycin MIC 2 mg L^{-1}) created from the same WT VREfm isolate as a comparison. Principal-

382 component analysis (PCA) of the detected lipids clearly separated the daptomycin-resistant
383 RpoB mutants from the WT and daptomycin-susceptible Q473L strain, indicating distinct lipid
384 profiles (Figure 5A). While the same classes of lipid species were observed in the WT and
385 daptomycin-resistant RpoB mutants, there were significant reductions in anionic cardiolipins
386 (CL) and phosphatidylglycerols (PG), as well as an increase in digalactosyldiacylglycerols
387 (DGDG) and cationic lysyl-PGs (Lys-PG) in the RpoB mutants (Figure 5B-E). CL, PG, DGDG, and
388 Lys-PG profiles returned to WT when each of the three RpoB mutations was reverted,
389 demonstrating that the differences observed in the daptomycin-resistant strains were due to
390 the RpoB substitutions (Supplementary Table 8).
391
392 Given the central role of RpoB in transcription, we hypothesised the lipidome differences of
393 the daptomycin-resistant RpoB mutants were caused by alterations in gene expression. We
394 firstly modelled the RNA polymerase complex structure in *E. faecium* to estimate the changes
395 imparted by Q473L, G482D, H486Y, and S491F substitutions on transcription at the protein
396 level. All four substitutions were present at the rifamycin active site and in direct interaction
397 with nucleic acids at the transcription replication fork, with predicted changes in stability or
398 altered interactions with nucleic acid templates (Supplementary Figure 10). The highly
399 prevalent S491F substitution defined changes to a bulkier hydrophobic side chain, with
400 predicted mild reductions in protomer stability and affinities to rifampicin, other RNA
401 polymerase subunits, and nucleic acids within the replication fork. Thereby suggesting that
402 even at objectively low reductions in affinity, this mutation can directly impact the
403 transcription rate, and the subsequent rate of gene expression. Conversely, the G482D
404 substitution resulted in the introduction of a bulkier negatively charged side chain, which led
405 to steric clashes and increased electrostatic potential of the RNA binding cleft. The G482D

406 substitution was predicted to have the largest detrimental effect on protein stability, which
407 may reduce the amount of active RNA polymerase and gene expression. Interestingly, it was
408 also predicted to increase nucleic acid binding affinity of the mutant complex, further reducing
409 RNA polymerase activity and processing. Finally, the daptomycin-resistant substitution H486Y
410 and daptomycin-susceptible substitution Q473L were predicted to confer similar effects to the
411 protein stability, and rifampicin and nucleic acid binding affinity. However, the H486Y
412 substitution, but not the Q473 substitution, was predicted to increase RNA polymerase
413 complex stability, reducing the dynamic flexibility required for enzyme activity, potentially
414 leading to the changes in gene expression. Overall, the daptomycin-resistant substitutions
415 S491F, H486Y, and G482D were all characterised by distinct interactions from the WT RNA
416 polymerase while the daptomycin-susceptible substitution Q473L retained the original WT
417 interactions.
418
419 Given the predicted changes in RNA polymerase transcriptional activity, we used a
420 combination of RNA sequencing (RNAseq) and data independent acquisition (DIA) based
421 proteomics and identified 26 loci that were significantly differentially expressed in both
422 RNAseq and proteomics in all three daptomycin-resistant strains (G482D, H486Y, and S491F),
423 but not in the daptomycin-susceptible strain (Q473L) or the WT VREfm (Figure 5F and
424 Supplementary Table 9). Of note, there was no differences in expression (by transcriptomics
425 or proteomics) of the *liaFSR*, *liaXYZ*, or *yycFG* (*walKR*) regulons or the cardiolipin synthase *(cls)*
426 or division site tropomyosin (*divIVA*) genes, indicating the mechanism of RpoB-mediated
427 daptomycin resistance was independent of previously described systems[10,11,21]. Since
428 compensatory *rpoC* mutations can alter the kinetic parameters of the RNA polymerase
429 enzyme, we hypothesised the number of dysregulated genes would decrease in the RpoBC

430 double mutant (RpoB S491F and RpoC T634K) compared to the single RpoB S491F mutant,
431 leaving genes likely associated with daptomycin resistance. Indeed, only six loci were
432 differentially expressed (by RNAseq and proteomics) in the RpoBC mutant, compared with 44
433 loci identified in the single RpoB S491F mutant (Figure 5F-G). These included genes encoding
434 a cold shock protein (CspA, [protein] AGS75480 or EFAU233_01583), a hypothetical protein of
435 unknown function, a potassium uptake transporter (K+ transporter, [protein] AGS74117 or
436 EFAU233_00176), and a DNA-binding transcriptional regulator of the PadR family in a putative
437 operon with two hypothetical membrane proteins ([proteins] AGS74325, AGS74326,
438 AGS74327 or EFAU233_00444, EFAU233_00445, EFAU233_00446). All six of these loci were
439 significantly upregulated (in RNAseq and proteomics) in the three daptomycin-resistant RpoB
440 mutants (G482D, H486Y, and S491F), as well as in the RpoBC double mutant.
441
442 To understand their potential role in daptomycin resistance, each of these six genes were
443 deleted from the WT and RpoB S491F mutant. The *dltC* gene, linked to daptomycin resistance
444 in *S. aureus*, was also included as it was differentially expressed in the G482D, H486Y, and
445 S491F strains, but not in the RpoBC double mutant. Deletion of *cspA*, *dltC*, the hypothetical
446 protein, or K+ uptake transporter did not alter daptomycin susceptibility in either the WT or
447 RpoB S491F backgrounds. However, deletion of the PadR-family regulator (named here *prdR*,
448 Phenotypic Resistance to Daptomycin Regulator) or individual deletions of the hypothetical
449 membrane proteins (named here *prdA* and *prdB*) increased daptomycin susceptibility by 4-
450 fold in the WT or S491F backgrounds (Figure 5H; Supplementary Figure 11A). Similar 4-fold
451 increases in daptomycin susceptibility were observed when these genes were deleted from
452 the RpoB G482D or H486Y backgrounds (Figure 5H).
453

454 Clinical paired VREfm isolates representative of the G482D, H486Y, and S491F mutations were
455 analysed by DIA proteomics to examine the abundance of PrdR, PrdA, and PrdB in the cell. In
456 daptomycin-resistant clinical strains carrying the S491F (ST1421 and ST203), G482D (ST80), or
457 H486Y (ST203) mutations, the production of PrdRAB was significantly (P<0.05) increased
458 compared to daptomycin-susceptible (WT *rpoB* allele) strains of the same ST (Supplementary
459 Figure 11B-C and Supplementary Table 9). The increased expression of PrdRAB in both
460 genetically distinct clinical VREfm harbouring the G482D, H486Y, or S491F mutations and in
461 isogenic strains, suggested the *prdRAB* operon was responsible for RpoB-mediated
462 daptomycin resistance.
463
464 **Upregulation of the *prdRAB* operon leads to cell membrane remodelling and decreased**
465 **daptomycin binding in daptomycin-resistant RpoB strains.**
466 We hypothesised the overexpression of the *prdRAB* operon in the RpoB mutants was leading
467 to the observed changes in the cell membrane and subsequent resistance to daptomycin.
468 Therefore, an overexpression vector with the *prdR* gene, along with an empty vector (EV)
469 control, were introduced separately into the WT VREfm. Consistent with this, plasmid
470 mediated overexpression of the *prdR* gene increased the WT daptomycin MIC 4-fold, to 8 mg
471 L^{-1}. Proteomic analysis (WT EV versus WT^{prdR}) confirmed the *prdR* regulator was expressed to
472 a similar level in the WT^{prdR} strain as in the RpoB mutants (2.5-fold and 2.2-fold in S491F,
473 respectively) and the *prdR* regulator specifically controlled the expression of the *prdAB*
474 membrane proteins (Supplementary Figure 12A and Supplementary Table 9). PCA of the WT,
475 WT EV, WT^{prdR}, and RpoB S491F lipidomes supported the overexpression of the *prdR* gene
476 driving the changes in the lipid species, with the WT^{prdR} and RpoB S491F lipidomes clustering
477 separately than the WT and WT EV lipidomes (Figure 6A and Supplementary Table 8).

478 Reductions in the same anionic phospholipids (CL and PG) and increases in cationic Lys-PG
479 species were observed in the WT^{prdR} strain to similar levels seen in the RpoB S491F mutant
480 (Figure 6B-C and Supplementary Figure 12B). Lipidomic analyses of the previously described
481 paired clinical isolates demonstrated the daptomycin-resistant clinical strains carrying RpoB
482 mutations had similar significant differences in charged phospholipids (decreases in CL and
483 PG, increases in Lys-PG), compared to daptomycin-susceptible strains containing the WT *rpoB*
484 allele (Figure 6D and Supplementary Table 8). These data indicated that overexpression of the
485 *prdRAB* operon in daptomycin-resistant VREfm carrying RpoB mutations leads to changes in
486 the abundance of charged lipid species in the cell membrane.
487
488 Given the decreases in anionic phospholipids (CL and PG) and increases in cationic
489 phospholipids (Lys-PG), we tested if strains harbouring RpoB mutations harbour differences in
490 overall cell membrane charge and daptomycin binding. As we predicted, both the daptomycin-
491 resistant isogenic and clinical RpoB mutants (G482D, H486Y, and S491F) had a significantly
492 reduced negative charge associated with the cell membrane compared to their paired isolate
493 (Figure 6E and Supplementary Figure 13A), respectively, and consequently bound less
494 fluorescent daptomycin (Figure 6F and Supplementary Figure 13C). Complementation of the
495 RpoB mutations reversed cell membrane charge and daptomycin binding to WT levels
496 (Supplementary Figure 13B and D). No significant difference was observed in membrane
497 charge or daptomycin binding for the daptomycin-susceptible Q473L strain (Figure 6E-F).
498 Further, the overexpression of the *prdR* gene resulted in a significantly reduced negative
499 charge across the cell membrane compared to the WT EV strain, with a similar charge to the
500 daptomycin-resistant RpoB mutants (Figure 6F). Additionally, binding of daptomycin was
501 significantly decreased compared to the WT EV strain (Figure 6F). These experiments show

502 that the increased expression of the *prdRAB* operon in VREfm carrying daptomycin resistance
503 associated RpoB mutations leads to changes in the abundance of charged phospholipids and
504 a decrease in the cell surface negative charge, which in turn reduces daptomycin binding to
505 the cell membrane.
506
507 **Discussion**
508 Here we show that specific amino acid substitutions within the RRDR of RpoB (G482D, H486Y,
509 and S491F) lead to clinical daptomycin resistance in *E. faecium*. These mutations are globally
510 distributed with prevalence equal to other well-characterised amino acid substitutions within
511 LiaFSR/LiaXYZ and Cls, which have been considered the dominant mechanisms of daptomycin
512 resistance in VREfm[21,38,39]. Although these findings are reminiscent of previous studies in *S.*
513 *aureus,* which have suggested that *rpoB* mutations can lead to reduced daptomycin
514 susceptibility, there are some important distinctions[40–42]. In *S. aureus, rpoB* mutations have
515 not been reported to result in clinical daptomycin resistance (defined as MIC≥ 2 mg L^{-1}), as
516 seen here in VREfm - rather they are associated with subtle changes in daptomycin
517 susceptibility. There are no reports in the literature of *rpoB* mutations leading to daptomycin
518 resistance in clinical *S. aureus* isolates, suggesting that *rpoB* mutations may be of limited
519 clinical importance to *S. aureus* daptomycin resistance. This contrasts with VREfm, where *rpoB*
520 mutations appear to be a major mechanism of daptomycin resistance. Through our multi-omic
521 approach we have defined the molecular mechanism by which *rpoB* mutations lead to
522 changes in daptomycin susceptibility in VREfm. Our analyses show that G482D, H486Y, and
523 S491F RpoB substitutions mediate daptomycin resistance via a conserved mechanism that is
524 independent of previously described systems (Lia operons or Cls). Each of these RpoB
525 substitutions caused similar transcriptional reprograming in VREfm, with dysregulation of a

526 previously uncharacterised genetic locus found to be responsible for daptomycin resistance.
527 The locus, that we have named the Phenotypic Resistance to Daptomycin (*prd*) operon
528 consists of a transcriptional regulator (PrdR) and two putative membrane proteins (PrdAB).
529 Upregulation of the *prdRAB* operon leads to cell membrane remodelling, with decreased
530 levels of anionic phospholipids (PG and CL) and increased levels of cationic phospholipids (Lys-
531 PG). This ultimately decreases the negative cell surface charge and reduces daptomycin
532 binding, which renders VREfm resistant to daptomycin. Notably, there was no dysregulation
533 of the *prdRAB* operon in an isogenic VREfm strain carrying an RpoB substitution (Q473L) that
534 did not confer daptomycin resistance and no membrane changes relative to the daptomycin-
535 susceptible WT were observed. The G482D, H486Y, and S491F RpoB substitutions studied here
536 should therefore be considered clinically relevant and major mediators of daptomycin
537 resistance in VREfm.
538
539 The S491F RpoB substitution in particular is common within the global *E. faecium* population,
540 being present in at least three phylogenetically distinct lineages currently circulating within
541 healthcare systems in Australia, the United Kingdom, the United States, and across Europe.
542 These lineages have spread over global geographic scales and persisted for at least 15 years,
543 which is of clinical concern since it suggests that they might eventually compromise the
544 therapeutic value of daptomycin for treating VREfm infections.
545
546 Exposure to rifamycin antimicrobials is a well-documented driver in the emergence of
547 bacterial strains carrying substitutions in RpoB, with mutations in this gene often leading to
548 high level rifamycin resistance[24]. In keeping with this, VREfm isolates carrying the G482D,
549 H486Y, and S491F RpoB substitutions are resistant to rifamycin antimicrobials in addition to

550 daptomycin, suggesting that rifamycin use might be an important driver in the emergence of
551 daptomycin-resistant VREfm. In support of this, our data suggests the clinical use of rifaximin
552 is likely responsible for driving VREfm isolates harbouring mutations within *rpoB* that are
553 cross-resistant to rifamycins and daptomycin. Three lines of evidence support this hypothesis:
554 (i) Bayesian phylodynamic analyses show the emergence of phylogenetically distinct VREfm
555 lineages carrying the S491F substitution is temporally linked with the clinical approval of
556 rifaximin in the early 2000s, with each lineage subsequently undergoing population expansion
557 following FDA approval in 2010 of rifaximin as a prophylactic for the prevention of hepatic
558 encephalopathy in chronic liver disease patients, (ii) two independent retrospective patient
559 cohort studies demonstrate that recent rifaximin exposure was predictive of carriage of
560 daptomycin-resistance RpoB substitutions, and (iii) animal experiments demonstrate the
561 administration of rifaximin to mice colonised with VREfm led to the *de novo* emergence of
562 VREfm strains within the gastrointestinal tract that carried substitutions within RRDR of RpoB
563 and were resistant to rifamycins and cross-resistant to daptomycin.
564
565 Although both rifaximin and rifampicin could drive the *de novo* emergence of daptomycin-
566 resistant VREfm in the mice experiments of our study, the data overall do not support a
567 prominent role for rifampicin in the emergence of daptomycin-resistant VREfm. This
568 hypothesis is based on a lack of temporal signal between the emergence of daptomycin-
569 resistant VREfm carrying RpoB substitutions (circa 2006) and the clinical introduction of
570 rifampicin which occurred in the early 1970s, as well as the observation that the vast majority
571 of daptomycin-resistant VREfm were only isolated from patients who received rifaximin in our
572 clinical analyses (and not from the control group). Why rifaximin appears to be a driver of
573 daptomycin resistance in *E. faecium* while rifampicin does not, is not immediately clear, but

574 may relate to the patient cohorts that rifampicin and rifaximin are primarily used to treat.
575 Rifaximin is used in patients with chronic liver disease who are recognised as one of the
576 highest risk groups for gastrointestinal VREfm carriage, while rifampicin and other rifamycins
577 are used in broader cohorts that are not frequently colonised with *E. faecium*. Our hypothesis
578 is that patients with chronic liver disease receiving rifaximin are a major source for the
579 emergence and subsequent spread of daptomycin-resistant VREfm carrying *rpoB* mutations.
580 Our analysis of the HSCT patient cohort demonstrates that this phenomenon is not restricted
581 to liver disease patients and is more generalisable, such that any patient colonised with VREfm
582 and receiving rifaximin is at risk of *E. faecium* carrying *rpoB* mutations that are daptomycin-
583 resistant emerging within the gut. There are some important clinical implications from this.
584 First, our results suggest that daptomycin should not be used for empiric therapy of invasive
585 VREfm infections in patients who are receiving rifaximin, or have recently received rifaximin,
586 given the significantly higher risk of daptomycin resistance. Secondly, to preserve the use of
587 daptomycin for VREfm, consideration should be given to maintaining isolation precautions in
588 hospitals for patients receiving rifaximin who are colonised with VREfm, avoiding cohorting
589 with other VREfm colonised patients where possible. Thirdly, although effective for
590 prophylaxis against hepatic encephalopathy, consideration should be given to keeping
591 rifaximin as a second-line option behind other therapies for this indication, and the use of
592 rifaximin for prophylaxis following HSCT reconsidered, given the propensity to induce
593 mutations in *rpoB* and subsequent daptomycin resistance.
594
595 There is a coordinated global effort to preserve the use of last-resort antimicrobials through
596 strict stewardship protocols that try to limit the use of these critically important medicines.
597 The rationale for this strategy assumes that restricted antibiotic usage equals less opportunity

598 for pathogens to develop resistance. Here we show that this assumption may be flawed, since
599 exposure to prophylactic rifaximin can lead to the emergence of daptomycin-resistant VREfm
600 in the absence of daptomycin exposure. These data highlight that unanticipated antimicrobial
601 cross-resistance can readily arise following the implementation of new antimicrobial regimes,
602 even when they are perceived to be "low-risk". Careful consideration should therefore be
603 given to the potential impact of prophylactic antibiotics on antimicrobial stewardship
604 practices.
605
606 We have identified a previously unrecognised, globally important mechanism of last-resort
607 antibiotic resistance in VREfm and show that prophylactic rifaximin use, particularly in chronic
608 liver disease patients, is a cause of this resistance. These findings demonstrate the ease with
609 which new antibiotic treatment regimens can drive the emergence of multidrug-resistant
610 pathogens and highlight the impact that unanticipated antibiotic cross-resistance can have on
611 antibiotic stewardship efforts designed to preserve the use of last-resort antibiotics. We
612 advocate for the judicious use of all antibiotics.
613

614 **Methods**

615 **Media and reagents**

616 *E. faecium* was routinely cultured at 37°C in brain heart infusion (BHI) broth (Becton Dickson)
617 or BHI agar (BHIA), BHI solidified with 1.5% agar (Becton Dickson). For electroporation, *E.*
618 *faecium* was cultured in BHI supplemented with 3% glycine and 200 mM sucrose (pH 7.0). *E.*
619 *coli* was cultured in Luria broth (LB). Broth microdilution (BMD) MICs were performed in
620 cation-adjusted Mueller Hinton with TES broth (CAMHBT) (Thermo Fisher). A concentration of
621 10 mg L^{-1} chloramphenicol (Sigma Aldrich) was used for plasmid selection in *E. faecium* and *E.*
622 *coli*. The following antibiotics were used at variable concentrations for susceptibility testing:
623 rifampicin (Sigma Aldrich), rifaximin (Sigma Aldrich), and daptomycin (Cubicin).
624 Oligonucleotides were purchased from Integrated DNA Technologies and are listed in
625 Supplementary Table 11. Plasmids were purified with Monarch Plasmid Miniprep Kit (NEB).
626 PCR products and gel extractions were purified using Monarch DNA Gel Extraction Kit (NEB).
627 Genomic DNA was purified using the Monarch Genomic DNA Purification Kit (NEB). Phusion
628 and Phire DNA polymerase was purchased from NEB.

629 **Bacterial isolates**

630 Bacterial strains used in this study are listed in Supplementary Table 10. Australian bacterial
631 strains were collected across three data projects in the Microbiological Diagnostic Unit Public
632 Health Laboratory (MDU PHL). Two unbiased cross-sectional surveys of VREfm were
633 conducted between 10 November and 9 December 2015 (n=331)[32] and between 1 November
634 and 30 November 2018 (n=323) in the State of Victoria (referred to as the 2015 and 2018
635 Snapshot). During this period, all VREfm-positive isolates (including screening and clinical
636 samples) collected by laboratories across the state were sent to the MDU PHL. In addition,
637 this project included *vanA*-VREfm collected from the "Controlling Superbugs" study[19,20], a 15-

638 month (April-June 2017 and October 2017-2018) prospective study including eight hospital
639 sites across four hospital networks, resulting in 346 VREfm isolates (308 patients) sent for WGS
640 at MDU PHL. The VREfm were isolated from patient samples (including screening and clinical
641 samples) routinely collected from hospital inpatients. For the 'historical *vanA*-VREfm,' every
642 *vanA* isolate collected within MDU PHL was included. This resulted in an additional 229
643 isolates, sampled between 2003 and 2014.
644 For publicly available isolates, our aim was to capture the diversity of *E. faecium* circulating
645 globally by including isolates that formed part of several key studies involving hospital-
646 associated VREfm (as of January 2021). To be included, isolates needed to have short-read
647 data available, with geographic location (by country), year of collection, and source (human
648 or animal). Reads were only included if they had a sequencing depth of >50x. To capture the
649 diversity of VREfm circulating in the United States, isolates from human sources were
650 downloaded from the PathoSystems Resource Integration Center[43]. All isolates were
651 confirmed to be *E. faecium* with the Kraken2 database (v.2.1.2)[44]. The final number of
652 international isolates comprised those from Africa (n=8), Asia (n=25), Europe (n=2941), North
653 America (n=424), and South America (n=78) (Supplementary Table 10).
654 **Antibiotic susceptibility testing**
655 Daptomycin susceptibility testing was performed using the BMD MIC method according to
656 CLSI guidelines. In a 96-well plate, a two-fold dilution series (from 32 to 0.5 mg L^{-1}) of
657 daptomycin was made in 100 μL volumes of CAMHBT, additionally supplemented with 50 mg
658 L^{-1} Ca^{2+}. An inoculum of 100 μL *E. faecium* broth culture adjusted to 1 x 10^6 CFU mL^{-1} in
659 CAMHBT was then added to each well. After 24 hours incubation, the MIC was defined as the
660 lowest antimicrobial concentration that inhibited visible growth. All assays were performed in
661 biological triplicate, with the median MIC reported. In accordance with recent guidelines[45],

662 isolates with a daptomycin MIC ≥ 8 mg L^{-1} were considered to be daptomycin-resistant. A
663 daptomycin-sensitive strain (AUS0085)[46] and a daptomycin-resistant strain (DMG1700661)[16]
664 were used as a control.
665 Rifampicin susceptibility testing was performed using the BMD method in CAMHBT. High-level
666 rifampicin resistance was defined with a MIC > 32 mg L^{-1}. All susceptibility testing was
667 performed in triplicate.

668 **Whole-genome sequencing**

669 Genomic DNA was extracted from a single colony using a JANUS automated workstation
670 (PerkinElmer) and Chemagic magnetic bead technology (PerkinElmer). Genomic DNA libraries
671 were prepared using the Nextera XT kit according to manufacturer's instructions (Illumina,
672 San Diego, CA, USA). Whole-genome sequencing was performed using Illumina NextSeq
673 platform, generating 150 bp paired-end reads. The short reads of isolates sequenced at MDU-
674 PHL are available on the NCBI Sequence Read Archive [BioProjects PRJNA565795 (Controlling
675 Superbugs), PRJNA433676 (2015 Snapshot) and PRJNA856406 (2018 Snapshot), and
676 PRJNA856406 (historical *vanA* isolates)].

677 **Phylogenetic analysis**

678 De novo assemblies of the genomes were constructed using Spades[47] (v3.13). In silico MLST
679 was determined using the program mlst with the efaecium database[48]
680 (https://github.com/tseemann/mlst). The 1000 Australian genomes as well as the 4,705
681 Australian and international VREfm were mapped to the reference *E. faecium* genome
682 AUS0085 isolated from a human bacteraemia infection in Victoria, Australia (NCBI accession:
683 CP006620)[46] using snippy (https://github.com/tseemann/snippy) (v4.4.5), applying a minfrac
684 value of 10 and mincov value of 0.9. This reference was selected as it was a publicly available
685 complete genome collected locally and daptomycin-susceptible. A maximum likelihood

686 phylogenetic tree was inferred using IQ-TREE (v2.1.2)[49] with a general time-reversible (GTR +
687 G4) substitution model, including invariable sites as a constant pattern and 1000 bootstrap
688 replicates. Recombination masking was not performed for species maximum likelihood trees
689 due to the small size of the resulting core alignment. All trees were mid-point rooted and
690 visualised in R (v4.0.3, https://www.r-project.org/) using phangorn[50] (v2.5.5), ape[51] (v5.4),
691 ggtree[52] (v2.3.4), and ggplot (v3.3.2).
692 The genome assemblies of all isolates were screened for acquired antimicrobial resistance
693 determinants using abriTAMR (https://github.com/MDU-PHL/abritamr)[53].

694 **Genome-wide association study of daptomycin resistance**

695 A GWAS approach was applied to identify genetic variants of daptomycin resistance in *E.*
696 *faecium*. A genotype matrix of SNPs was constructed and used as input to homoplasyFinder[54]
697 (v0.0.0.9) to determine the consistency index at each locus and kept mutations that had an
698 index of ≤0.5 (indicating at least two independent acquisitions across the phylogeny). We then
699 ran GWAS using daptomycin resistance as a binary trait, where isolates were categorised as
700 resistant if their daptomycin MIC was ≥8 mg L^{-1}. To correct for population structure, we used
701 the factored spectrally transformed linear mixed models (FaST-LMM) implemented in pyseer[55]
702 (v.1.3.6), which computes a kinship matrix based on the core genome SNPs as a random effect.
703 *P* values were corrected for multiple hypothesis testing using the Bonferroni correction
704 method.

705 **Competition assay**

706 For competition assays, overnight cultures of WT and corresponding RpoB S491F or RpoB
707 S491F/RpoC T634K mutants were diluted to an OD600 of 0.5 in BHI and equal volumes added
708 to an overnight culture. Serial dilutions of each co-culture were performed at times 0 and 24

709 hours on BHIA. Colonies were then replica plated onto BHIA and BHIA rifampicin 20 µg mL^{-1}
710 to determine the proportion of WT to mutant.

711 **Core genome MLST (cgMLST) and clustering**

712 cgMLST alleles for each isolate was defined using the public *E. faecium* cgMLST scheme[56] and
713 chewBBACA (v2.0.16)[57], implemented locally in the COREugate pipeline (v2.0.4)
714 (https://github.com/kristyhoran/Coreugate). The pipeline determines the alleles of each core
715 gene for every isolate as defined by the specific pathogen scheme. The *E. faecium* cgMLST
716 scheme contains 1,423 genes. The number of allelic differences between each isolate within
717 this core set of genes is then determined. The cgMLST clusters were determined using single
718 linkage clustering and a pairwise allelic difference threshold of ≤250. This threshold was
719 chosen since it maximised diversity within clusters, to improve temporal sampling depth,
720 while still clustering based on maximum-likelihood tree structure.

721 **Phylodynamic analyses of the emergence of the S491F RpoB mutation in VREfm lineages**

722 To investigate the emergence of the S491F mutation in RpoB in three different lineages, as
723 defined with cgMLST, we undertook further analysis on these clusters/lineages. From the
724 species-level maximum-likelihood tree (Figure 2C), three lineages/clusters were identifiable
725 by cgMLST due to their size (n>50) and presence of the S491F mutation. The three clusters
726 were analysed independently, such that individual core-genome SNP alignments were
727 generated, since this increased the length of the core alignment and number of sites
728 considered. Snippy (https://github.com/tseemann/snippy) (v4.4.5) was used to generate the
729 alignments for each cluster to the corresponding reference genome
730 (AUSMDU00004024/CP027517.1 for Cluster 1, AUSMDU00004055/CP027506.1 for Cluster 2,
731 and AUSMDU00004142/CP027501.1 for Cluster 3). Each core alignment used a within 'cluster
732 reference' (complete genome of the same cluster) to maximise core-SNP alignment length.

733 The reference for each cluster was chosen since they were a locally-collected, closed genome.
734 Recombination was removed from the final alignment using Gubbins[58] (v.2.4.1) to ensure
735 modelling was only informed by SNPs with tree-like evolution within the core genome.
736 Maximum-likelihood trees for each of the three clusters were inferred from the core-SNP
737 alignments [Cluster 1: (n=219 taxa) 329 SNPs; Cluster 2: (n=85 taxa) 541 SNPs; Cluster 3: (n=68
738 taxa) 764 SNPs] with IQ-tree (v2.1.2)[59] with a general time-reversible (GTR+G4) substitution
739 model, including invariable sites as a constant pattern. Phylogenetic uncertainty was
740 determined through 1000 nonparametric bootstrap replicates.
741 To investigate temporal signal in the three clusters of VREfm genomes, we first used TempEst[60]
742 (v1.5). A root-to-tip regression analysis was performed on the root-to-tip branch distances
743 within the three, cluster maximum-likelihood phylogenies as a function of year of collection,
744 with the position of the root optimised according to the heuristic residual mean squared
745 method.
746 The frequency of the emergence of the *rpoB* mutation in VREfm was inferred using a discrete
747 trait model implemented in BEAST[61] (v1.10.4). Under this model the SNP alignments are used
748 to infer the evolutionary process (i.e. phylogenetic tree, time, and nucleotide substitution
749 model parameters) for the three clusters. The alignments all shared the HKY substitution
750 model and a constant-size coalescent population prior[26]. To avoid ascertainment bias due to
751 using a SNP alignment, the number of constant sites were considered for the likelihood
752 calculations. The molecular clock was a relaxed clock with an underlying lognormal
753 distribution. The molecular clock was calibrated using isolation dates for each genome by year
754 of collection and the mean clock rate is shared between all three alignments, but the model
755 allows for the individual alignments to have different standard deviations of the lognormal
756 distribution and also different branch rates. The mean molecular clock rate requires an explicit

757 prior distribution, for which we used a Gamma distribution and a 0.95 quantile range of
758 $4.9x10^{-6}$ and $1.1x10^{-4}$ substitutions/site/year. This informative prior means that it acts as an
759 additional source of molecular clock calibration.
760 The presence or absence of the S491F mutation in *rpoB* was used as a binary trait[62,63]. The
761 trait model was shared between the three alignments, with the different Markov jumps and
762 rewards (i.e. changes of trait state and time spent in each state, respectively) recorded for
763 each of the three alignments. The posterior distribution of model parameters was sampled
764 using a Markov chain Monte Carlo of 100,000,000 iterations, sampling every 100,000
765 iterations. Two independent runs were run for the models. We assessed sufficient sampling
766 from the stationary distributions by verifying the effective sample size of key parameters was
767 around or above 200. The final maximum-clade credibility trees were visualised in R (v4.0.3,
768 https://www.r-project.org/) using ggtree[52] (v2.3.4). The Markov jumps for the *rpoB* trait for
769 each alignment were visualised in R (v4.0.3, https://www.r-project.org/).
770 **Construction of isogenic mutants using allelic exchange and of pRAB11*prdR***
771 The *rpoC*^{T634K}, *rpoB*^{G482D}, *rpoB*^{H486Y}, *rpoB*^{S491F}, *rpoB*^{Q473L} , ABC transporter (I274S), permease
772 protein (G71S), or mannitol dehydrogenase (V288L) mutations were recombined into the
773 chromosomal copy of each gene in ST796 VREfm (Ef_aus0233) by allelic exchange. Deletions
774 of the CpsA, K+ transporter, hypothetical protein, DltC, or PrdRAB were also completed using
775 allelic exchange. The region encompassing each gene was amplified by SOE-PCR and
776 recombined into pIMAY-Z[64] by the seamless ligation cloning extract (SLiCE)[65] method and
777 transformed into *E. coli* IM08B[64]. The construct was transformed into electrocompetent
778 VREfm[65], with allelic exchange performed as described previously[66]. Reversion of *rpoB*^{G482D},
779 *rpoB*^{H486Y}, or *rpoB*^{S491F} mutations were completed using allelic exchange with a construct
780 containing the respective wild-type allele. To construct a vector containing *prdR*, the vector

781 pRAB11 was used. The *prdR* gene was amplified using Aus0233 genomic DNA. The *prdR*
782 product was gel extracted, SLiCE cloned into amplified pRAB11, and transformed into IMO8B,
783 yielding pRAB11:*prdR*. The plasmid and empty vector was then electroporated into Aus0233.
784 Genome sequencing and analysis of all mutants was conducted as described, with resulting
785 reads mapped to the Ef_aus0233 reference genome and mutations identified using Snippy
786 (https://github.com/tseemann/snippy) (v4.4.5).

787 **VREfm *in vivo* gastrointestinal colonisation experiments**

788 Female C57BL/6 mice at 6-8 weeks of age were purchased from WEHI and maintained in a
789 specific-pathogen-free facility at the Peter Doherty Institute for Infection and Immunity. All
790 animal handling and procedures were performed in a biosafety class 2 cabinet. Animal
791 procedures were performed in compliance with the University of Melbourne guidelines and
792 approved by the University's Animal Ethics Committee.

793 The dose for each antibiotic was calculated using the FDA human conversion formula to
794 ensure each mouse was given a human-equivalent dose[67]. To establish gastrointestinal
795 colonisation of VREfm, mice were administered ceftriaxone (410 mg kg^{-1} day^{-1}; AFT
796 Pharmaceuticals) via subcutaneous injection once daily for 4 days, followed by an antibiotic
797 wean period of 24 hours. Mice were then inoculated with 10^6 VREfm in 100 μl PBS by oral
798 gavage. Three days after VREfm inoculation, single-housed mice were administered either
799 rifaximin (113 mg kg^{-1} administered twice daily; Sigma Aldrich), rifampicin (123 mg kg^{-1}
800 administered once day; Sigma Aldrich), or vehicle (Corn oil with 10% DMSO) via oral gavage;
801 or daptomycin (50 mg kg^{-1} administered once daily; Cubicin) via subcutaneous injection [this
802 results in similar exposure (AUC_{0-24}) to that observed in humans receiving 8 mg kg^{-1} of
803 intravenous daptomycin[68]]. The above antibiotic dosing protocol was followed for 7 days.
804 Faecal samples were collected at specific time points throughout the experiment to determine

805 VREfm gut colonisation and for downstream rifamycin and daptomycin resistance analysis.
806 Faecal samples were resuspended in PBS to a normalised concentration (100 mg ml^{-1}). Serial
807 dilutions were performed, and samples were plated onto Brilliance VRE agar (Thermo Fisher)
808 for VREfm CFU enumeration.
809 For rifamycin and daptomycin analysis, VREfm colonies (n=50 per mouse) from the Brilliance
810 VRE agar plates were replica plated onto BHIA with and without rifampicin 20 µg mL^{-1} to
811 determine the proportion of rifampicin-resistant VREfm in each mouse. Fifty colonies per
812 mouse were then screened for daptomycin resistance, with a single colony being resuspended
813 in PBS, then diluted 1/100 into CAMHBT containing 50 mg L^{-1} Ca^{2+}, and 1/100 in CAMHBT
814 containing 50 mg L^{-1} Ca^{2+} and 8 mg L^{-1} daptomycin. All suspected daptomycin-resistant
815 colonies were confirmed using a daptomycin BMD MIC as before.
816 To determine which mutations were present in the rifamycin-resistant isolates, a random
817 selection of 300 colonies, 150 from rifaximin treated mice and 150 from rifampicin treated
818 mice (50 pre and 100 post for each treatment), were sampled for WGS as described above.
819 **Analysis of patients receiving rifaximin for hepatic encephalopathy prophylaxis.**
820 To examine the potential association between rifaximin exposure and daptomycin-resistant
821 VREfm, we analysed VREfm collected between 2014 and 2022 from a single quaternary
822 hospital institution in Melbourne. 225 patients were assessed for previous exposure to
823 rifaximin, which was defined as at least a single dose administered prior to the collection date
824 for the VREfm isolate, and grouped into “Rifaximin-exposed” and unexposed “Control” groups.
825 Only a single isolate was selected at random for testing and analysis from patients who had
826 multiple samples with VREfm isolates. The VREfm isolates underwent WGS and daptomycin
827 and rifampicin susceptibility testing as before. Patients with VREfm isolates that were assessed
828 as genetically clustered with other VREfm isolates in the cohort and likely represented direct

829 transmission were excluded. Genetic clustering was defined using an international standard
830 SNP cut-off (7 SNPs)[69,70] using a split Kmer (k=15) analysis (SKA)
831 (https://github.com/simonrharris/SKA) (v.1.0), a reference-free pairwise method that
832 compares the entire genome (unlike traditional core-genome based comparisons). Medical
833 records from patients were reviewed for comorbidity and antibiotic prescribing data. Potential
834 associations were assessed through univariate analysis using Pearson's chi-squared test or
835 Fisher's exact test for categorical data, and the Student's *t*-test (parametric) or Wilcoxon Rank
836 Sum test (non-parametric) for continuous data. To determine predictors of daptomycin-
837 resistant VREfm, multivariable logistic regression with backward stepwise elimination
838 procedure was used, excluding variables with $P>0.10$ and re-including variables with $P<0.05$.
839 Exposure to rifampicin and daptomycin were forced into the models as variables *a priori*. A *P*
840 value of <0.05 was considered statistically significant. Cases with missing data (e.g. incomplete
841 medical records data due to inter-hospital transfer) were excluded. Several sensitivity analyses
842 were also performed to assess for independent associations after excluding potential
843 confounders, including analysis with exclusion of variables with <10 outcomes, assessing
844 associations with antimicrobial exposure separately from demographic and comorbidity data,
845 and modifying the rifaximin exposure variable to include a) any prior exposure to rifaximin
846 (including both recent and distant exposure), and b) any prior exposure to rifamycin antibiotics
847 (including rifampicin, rifabutin and rifaximin). The genomic relationships of VREfm isolates
848 were visualised in a maximum-likelihood phylogenetic tree as before, using a core-SNP
849 alignment of 12886 sites. The mutations in RpoB were determined using snippy
850 (https://github.com/tseemann/snippy) (v4.4.5) as described.

851 **Analysis of patients receiving rifaximin for haematopoietic stem cell transplantation**
852 **prophylaxis.**

853 To examine the potential association between rifaximin exposure and the presence of
854 daptomycin associated *rpoB* substitutions in VREfm independent of underlying chronic liver
855 disease, we analysed isolates collected from patients undergoing haematopoietic stem cell
856 transplantation (HSCT) from a hospital institution in Regensburg, Germany. In this cohort,
857 rifaximin is used for gut decontamination to reduce risk of gastrointestinal graft-versus-host-
858 disease, while liver cirrhosis is a contraindication to HSCT. There were 68 patients initially
859 assessed for recent exposure to rifaximin, which was defined as at least a single dose
860 administered within 90 days prior to the isolate collection date. Only a single isolate was
861 retained for testing and analysis from patients who had multiple samples. In this instance, the
862 isolate included was randomised. The isolates underwent WGS using Ion Torrent Next-
863 Generation sequencing technology (Thermo Fisher) and nanopore (Oxford Nanopore).
864 Patients with isolates that were assessed as genetically clustered with other isolates in the
865 cohort and likely represented direct transmission were excluded (as above). Statistical and
866 phylogenetic analyses were undertaken as described above.

867 **Ultrahigh-performance liquid chromatography (UHPLC) and mass spectrometry (MS)**
868 **analyses**

869 Cultures of VREfm (n=5) were grown to mid-exponential phase (OD600 = 0.6) and washed in
870 PBS. The protein content for each sample was measured with a Pierce BCA Protein Assay Kit
871 (Thermo Fischer) and normalised to 100 μg. Cells were lysed using Bertin Precellys 24
872 homogenizer set at 6000 rpm for 40 seconds and lipids were subjected to monophasic
873 extraction as described previously[72]. Lipidomic samples were analysed by UHPLC coupled to
874 tandem mass spectrometry (MS/MS) employing a Vanquish UHPLC linked to an Orbitrap
875 Fusion Lumos mass spectrometer (Thermo Fisher Scientific, San Jose, CA, USA), with separate
876 runs in positive and negative ion polarities. Solvent A [60:40 (v:v) acetonitrile/water with 5

877 mM medronic acid and 10 mM ammonium acetate] and solvent B [90:10 (v:v)
878 isopropanol:acetonitrile with 10 mM ammonium acetate]. 10 µL of each sample was injected
879 into an Acquity UPLC HSS T3 C18 column (1 x 150 mm, 1.8 µm; Waters, Milford, MA, USA) at
880 50 °C at a flow rate of 60 µL/min for 3 min using 3% solvent B. During separation, the
881 percentage of solvent B was increased from 3% to 70% in 5 min and from 70% to 99% in 16
882 min. Subsequently, the percentage of solvent B was maintained at 99% for 3 min. Finally, the
883 percentage of solvent B was decreased to 3% in 0.1 min and maintained for 3.9 min.
884 All MS experiments were performed using an electrospray ionization source. The spray
885 voltages were 3.5 kV in positive ionisation-mode and 3.0 kV in negative ionisation-mode. In
886 both polarities, the flow rates of sheath, auxiliary and sweep gases were 25 and 5 and 0
887 arbitrary unit(s), respectively. The ion transfer tube and vaporizer temperatures were
888 maintained at 300 °C and 150 °C, respectively, and the ion funnel RF level was set at 50%. In
889 the positive ionisation-mode from 3 to 24 min, top speed data-dependent scan with a cycle
890 time of 1 s was used. Within each cycle, a full-scan MS-spectra were acquired firstly in the
891 Orbitrap at a mass resolving power of 120,000 (at m/z 200) across an m/z range of 300–2000
892 using quadrupole isolation, an automatic gain control (AGC) target of 4e5 and a maximum
893 injection time of 50 milliseconds, followed by higher-energy collisional dissociation (HCD)-
894 MS/MS at a mass resolving power of 15,000 (at m/z 200), a normalised collision energy (NCE)
895 of 27% at positive mode and 30% at negative mode, an m/z isolation window of 1, a maximum
896 injection time of 35 milliseconds and an AGC target of 5e4.
897 **Identification and quantification of lipids and statistical analysis**
898 LC-MS/MS data was searched through MS Dial 4.90. The mass accuracy settings were 0.005
899 Da and 0.025 Da for MS1 and MS2. The minimum peak height was 50000 and mass slice width
900 was 0.05 Da. The identification score cut off was 80%. In positive ionisation mode, [M+H]+,

901 [M+NH4]+ and [M+H-H2O]+ were selected as ion forms. In negative ionisation mode, [M-H]-
902 and [M+CH3COO]- were selected as ion forms. All lipid classes available were selected for the
903 search. PC, Lys-PC, DG, TG, CE, SM were identified and quantified from positive ionisation
904 mode while PE, LPE, PS, LPS, PG, LPG, PI, LPI, PA, LPA, Cer, CL were identified and quantified in
905 negative ionisation mode. The retention time tolerance for alignment was 0.1 min. Lipids with
906 maximum intensity less than 5-fold of average intensity in blank were removed. All other
907 settings were default. All lipid LC-MS features were manually inspected and re-integrated
908 when needed. These four types of lipids, 1) lipids with only sum composition except SM, 2)
909 lipid identification due to peak tailing, 3) retention time outliner within each lipid class, 4) LPA
910 and PA artefacts generated by in-source fragmentation of LPS and PS were also removed. The
911 shorthand notation used for lipid classification and structural representation follows the
912 nomenclature proposed previously[73]. Relative quantification of the lipid species was achieved
913 using the mass spectrometry intensity of each lipid ion at apex of LC peak and normalized to
914 the protein quantity in each sample.

915 **RNA-seq transcriptomics analysis**

916 Cultures were grown to mid-exponential phase (OD600 = 0.6) and total RNA was extracted
917 using Direct-zol RNA Miniprep kit (Zymo Research) according to manufacturer's instructions.
918 Cells were lysed using Bertin Precellys 24 homogenizer set at 6000 rpm for 40 seconds.
919 Samples were treated with TURBO DNase (Thermo Fisher) followed by clean up with the RNA
920 clean and concentrator kit (Zymo Research) according to manufacturer's instructions. The
921 absence of DNA contamination was checked by PCR and RNA integrity and purity was checked
922 with a Bioanalyser RNA kit (Agilent). Five sequencing libraries from independent RNA
923 extractions were made for each of the VREfm strains using the Stranded Total RNA with Ribo-
924 Zero Plus (Illumina) kit and sequenced on a single lane of an Illumina NovaSeq 6000 platform.

925 Raw paired-end reads were quality trimmed using TrimGalore
926 (https://www.bioinformatics.babraham.ac.uk/projects/trim_galore/) (v0.6.2). Bases with a
927 quality score <20 and reads shorter than 50bp after trimming were discarded. rRNA was
928 removed by the BBDuk script in BBtools (https://sourceforge.net/projects/bbmap/) (v39.01).
929 The resulting reads were aligned to the Aus0233 reference genome by Bowtie2[74] (v2.5.1)
930 using the --no-mixed flag and read counts were generated using htseq-count[75] (v. 0.12.4) using
931 the options -r pos -t CDS -m union --nonunique none. Differentially expressed genes were
932 detected using Degust (v4.1.1). Genes with $\log_2$(fold change) >1.5 and adjusted p-value < 0.05
933 were considered differentially expressed.

934 **Proteomic analysis**

935 Pelleted snap frozen bacterial cells (OD600 = 0.6) were solubilized in 4% SDS, 100mM Tris pH
936 8.5 by heating them for 10 min at 95 °C. The protein concentrations were assessed by a
937 bicinchoninic acid protein assay (Thermo Fisher Scientific) and 100 µg of each biological
938 replicate prepared for digestion using Micro S-traps (Protifi, USA) according to the
939 manufacturer's instructions. Briefly, samples were reduced with 10mM DTT for 10 mins at
940 95°C and then alkylated with 40mM IAA in the dark for 1 hour. Samples were acidified to 1.2%
941 phosphoric acid and diluted with seven volumes of S-trap wash buffer (90% methanol, 100
942 mM tetraethylammonium bromide pH 7.1) before being loaded onto S-traps and washed 3
943 times with S-trap wash buffer. Samples were then digested with trypsin before being collected
944 by centrifugation after the addition of 100 mM tetraethylammonium bromide, followed by
945 0.2% formic acid and then 0.2% formic acid / 50% acetonitrile. Samples were dried and further
946 cleaned up using C18 Stage[76,77] tips to ensure the removal of any particulate matter.

947 C18 enriched proteome samples were re-suspended in 2% acetonitrile (aq) containing 0.01%
948 trifluoroacetic acid (Buffer A*) and separated using a Vanquish Neo UHPLC (Thermo Fisher

949 Scientific) with a single column chromatography set up composed of a ACQUITY UPLC Peptide
950 BEH C18 Column (300Å, 1.7 µm, 1 mm X 100 mm, Waters Corporation) at a flow rate of 50
951 µL/min. Proteome samples were loaded directly on to the ACQUITY column with Buffer A
952 (0.1% formic acid, 2% DMSO) coupled directly to an Orbitrap 480™ mass spectrometer
953 (Thermo Fisher Scientific) and the buffer composition altered from 2% Buffer B (0.1% formic
954 acid, 77.9% acetonitrile, 2% DMSO) to 26% B over 70 minutes, then from 26% B to 99% B over
955 2 minutes and then was held at 99% B for 1.5 minutes. The mass spectrometer was operated
956 in a data-independent mode automatically switching between the acquisition of a single
957 Orbitrap MS scan (370-1050 m/z, maximal injection time of 50 ms, an AGC set to a maximum
958 of 300% and mass resolving power of 120,000 (at m/z 200) and the collection of 16.5 m/z DIA
959 windows between 375 and 1015 m/z (200-2000 m/z, NCE 32%, maximal injection time of 54
960 ms, an AGC set to 1000% and a mass resolving power of 30,000 (at m/z 200). Identification
961 and label free quantitation (LFQ) analysis were accomplished using Spectronaut (Biognosys,
962 Switzerland) versions 16 (16.0.220606.53000) using directDIA based analysis with minor
963 modifications: Protein LFQ method set to MaxLFQ, single hit proteins excluded, and
964 imputation disabled. Data was searched against the *E. faecium* Aus0004 proteome[46] (Uniprot
965 accession: UP000007591) with Carbamidomethyl (C) allowed as a fixed modification and
966 Acetyl (Protein N-term) as well as Oxidation (M) allowed as variable modifications. Data
967 outputs from Spectronaut were processed using Perseus (version 1.6.0.7)[78] with missing
968 values imputed based on the total observed protein intensities with a range of 0.3 σ and a
969 downshift of 1.8 σ. Statistical analysis was undertaken in Perseus using two-tailed unpaired *t*-
970 tests and ANOVAs. Proteins with $\log_2$(fold change) >1 and adjusted p-value < 0.05 were
971 considered differentially expressed.

972 **Computational modelling**

973 In predicting the potential effects of substitutions Q473L, G482D, H486Y, and S491F, the full *E.*
974 *faecium* DNA-dependent RNA polymerase was initially modelled using Advanced Homology
975 Modelling in Maestro (Schrodinger suite). BLAST-pdb was used to identify the *M. tuberculosis*
976 homologue (PDB: 5UHC)[36] as the template, as it had the best sequence identities across all
977 RNA polymerase subunits. Modelling was carried out based on consensus between sequence
978 alignments from MAFFT-DASH[79], T-COFFEE[80], and Clustal-W[81] (within Maestro), which were
979 manually optimised to minimise sequence gaps. The final RNA polymerase model, bound to
980 rifampicin and the DNA replication fork was next subjected to loop refinement and
981 minimisation, and iteratively assessed for model quality within Maestro.
982 The modelled structure was used as input within *in silico* biophysical predictors Dynamut2[82],
983 mmCSM-lig (https://biosig.lab.uq.edu.au/mmcsm_lig/), mmCSM-NA[83], and mCSM-PPI2[83],
984 which predicted the effects of mutations Q473L, G482D, H486Y, and S491F on β-subunit
985 stability, and affinities to rifampicin, nucleic acids within the replication fork, and other RNA
986 polymerase subunits, respectively. During interpretation, all values were collectively
987 considered to assess potential protein-level implications to wild type function. In doing so, the
988 affinity values for mutations located beyond 12 Å of the binding partner were presumed
989 negligible.
990 **Estimation of Zeta potential**
991 The Zeta potential was measured on cells grown to exponential phase (OD600 = 0.6) and
992 washed in PBS. The Zeta potential measurements were performed in PBS to minimise
993 influence of pH. Each experiment was carried out under identical experiment conditions (n=5),
994 25°C with two minutes of equilibration. The Zeta potential was measured with a Zetasizer
995 (Malvern, UK).
996 **Determination of cell-associated daptomycin with BoDipy labelling**

997 BoDipy fluorescent dye (4,4-Difluoro-1,3,5,7,8-Pentamethyl-4-Bora-3a,4a-Diaza-S-Indacene)
998 (Invitrogen) was used to label daptomycin with minor modifications[84]. Briefly, 50 µL
999 daptomycin (50 mg mL^{-1}) was mixed with 100 µL BoDipy (10 mg mL^{-1}) and was made up to a
1000 final volume of 1 mL in 200 mM sodium bicarbonate (pH 8.5). The reaction was incubated for
1001 1 hour at 37°C and unbound BoDipy was removed by dialysis at 4°C using a Slide-A-Lyzer
1002 cassette (Thermo Scientific), with a 2.0 kDa cut-off, as per manufacturer's instructions. The
1003 antibiotic activity of BoDipy-daptomycin was confirmed by BMD (described above). To
1004 measure cell-associated DAP, cultures were grown to exponential phase (OD600 = 0.6) 50 mg
1005 L^{-1} $CaCl_2$. Each culture was incubated with BoDipy-daptomycin in darkness (10 minutes) and
1006 washed to remove unbound BoDipy- daptomycin. The amount of bound BoDipy- daptomycin
1007 was measured with excitation at 490 nm and emission at 528 nm using an Ensight microplate
1008 reader (PerkinElmer). Biological replicates (n=5) were completed on separate days.

1009 **Data visualisation and statistics**

1010 All figures were generated in R (v4.0.3, https://www.r-project.org/) using tidyverse (v.1.3.1),
1011 patchwork (v.1.1.1), and ggnewscale (v.0.4.5). Statistical analyses were performed using R
1012 (v4.0.3, https://www.r-project.org/) and GraphPad Prism (v9.3.1) software packages. Specific
1013 tests are provided together with each corresponding result in the text.

1014 **Ethics approval**

1015 Data were obtained from medical records with approval from the local Human Research Ethics
1016 Committee (HREC/92972/Austin-2023).

1017 **Competing Interests**

1018 The authors declare no competing interests.

1019 **Acknowledgements**

1020 This work was supported by the National Health and Medical Research Council (NHMRC) of
1021 Australia (GNT1185213 and GNT1160745). BPH is supported by an NHMRC Investigator Grant
1022 (GNT1196103). JCK is supported by an NHMRC Early Career Fellowship (GNT1142613). AMT
1023 and NLS are supported by an Australian Government Research Training Program scholarship.
1024 DJI is supported by an NHMRC Investigator Grant (GNT1195210). SD is supported by the
1025 Australian Research Council (DE190100805). The Controlling Superbugs study was supported
1026 by the Melbourne Genomics Health Alliance (funded by the State Government of Victoria,
1027 Department of Health and Human Services, and the 10 member organizations). NES is
1028 supported by an Australian Research Council Future Fellowship (FT200100270) and an ARC
1029 Discovery Project Grant (DP210100362). We thank the Melbourne Mass Spectrometry and
1030 Proteomics Facility of The Bio21 Molecular Science and Biotechnology Institute for access to
1031 MS instrumentation and staff within the Microbiological Diagnostic Unit Public Health
1032 Laboratory for technical assistance with antimicrobial susceptibility testing and whole genome
1033 sequencing.

1034 **Author Contributions**

1035 GPC, BPH, and CLG conceived and planned the experiments. AMT, LL, IRM, DJI, SD, SP, NI, LKS,
1036 GR, SN, NES, BAE, DA, and GPC performed the planned experiments. JCK, NEH, BK, DW, AG
1037 and EH provided access to necessary patient metadata and JCK and SV preformed statistical
1038 analyses in the patient cohort studies. AH, JYHL, NLS, TPS, TS, BPH, EH and JCK provided critical
1039 clinical or bioinformatic insights for the study. AMT, CLG, and GPC co-wrote the manuscript
1040 with critical feedback and input from all authors.

1041 **Corresponding Authors**

1042 Correspondence to Glen Carter or Benjamin Howden.

1043 **Data Availability**

The WGS and RNA sequencing data presented in the study are deposited under Bioprojects PRJNA565795, PRJNA433676, PRJNA856406, and PRJNA856406. The mass spectrometry proteomics data has been deposited in the Proteome Xchange Consortium via the PRIDE partner repository[85] with the data set identifier: PXD039832 (Username: reviewer_pxd039832@ebi.ac.uk Password: fwjEy0ah) and PXD039831 (Username: reviewer_pxd039831@ebi.ac.uk Password: 9SrIrmu8).

1051 **References**

1052 1. Murray, C. J. *et al.* Global burden of bacterial antimicrobial resistance in 2019: a
1053 systematic analysis. *The Lancet* **399**, 629–655 (2022).
1054 2. Bylicka-Szczepanowska, E. & Korzeniewski, K. Asymptomatic Malaria Infections in the
1055 Time of COVID-19 Pandemic: Experience from the Central African Republic. *Int. J.*
1056 *Environ. Res. Public. Health* **19**, 3544 (2022).
1057 3. Global HIV & AIDS statistics — Fact sheet. https://www.unaids.org/en/resources/fact-
1058 sheet.
1059 4. GBD 2019 Collaborators. Global mortality from dementia: Application of a new method
1060 and results from the Global Burden of Disease Study 2019. *Alzheimers Dement. N. Y. N* **7**,
1061 e12200 (2021).
1062 5. Arias, C. A. & Murray, B. E. The rise of the *Enterococcus*: beyond vancomycin resistance.
1063 *Nat. Rev. Microbiol.* **10**, 266–278 (2012).
1064 6. Top, J., Willems, R. & Bonten, M. Emergence of CC17 *Enterococcus faecium*: from
1065 commensal to hospital-adapted pathogen. *FEMS Immunol. Med. Microbiol.* **52**, 297–308
1066 (2008).
1067 7. Arthur, M. & Courvalin, P. Genetics and mechanisms of glycopeptide resistance in
1068 enterococci. *Antimicrob. Agents Chemother.* **37**, 1563–1571 (1993).
1069 8. De Oliveira, D. M. P. *et al.* Antimicrobial Resistance in ESKAPE Pathogens. *Clin. Microbiol.*
1070 *Rev.* **33**, e00181-19 (2020).
1071 9. Tacconelli, E. *et al.* Discovery, research, and development of new antibiotics: the WHO
1072 priority list of antibiotic-resistant bacteria and tuberculosis. *Lancet Infect. Dis.* **18**, 318–
1073 327 (2018).

1074 10. Montero, C. I., Stock, F. & Murray, P. R. Mechanisms of Resistance to Daptomycin in
1075 *Enterococcus faecium*. *Antimicrob. Agents Chemother.* (2008) doi:10.1128/AAC.00774-
1076 07.
1077 11. Diaz, L. *et al.* Whole-Genome Analyses of *Enterococcus faecium* Isolates with Diverse
1078 Daptomycin MICs. *Antimicrob. Agents Chemother.* (2014).
1079 12. Lellek, H. *et al.* Emergence of daptomycin non-susceptibility in colonizing vancomycin-
1080 resistant *Enterococcus faecium* isolates during daptomycin therapy. *Int. J. Med.*
1081 *Microbiol.* **305**, 902–909 (2015).
1082 13. Kelesidis, T., Tewhey, R. & Humphries, R. M. Evolution of high-level daptomycin
1083 resistance in *Enterococcus faecium* during daptomycin therapy is associated with limited
1084 mutations in the bacterial genome. *J. Antimicrob. Chemother.* **68**, 1926–1928 (2013).
1085 14. Werth, B. J. *et al.* Defining Daptomycin Resistance Prevention Exposures in Vancomycin-
1086 Resistant *Enterococcus faecium* and *E. faecalis*. *Antimicrob. Agents Chemother.* **58**,
1087 5253–5261 (2014).
1088 15. Turner, A. M., Lee, J. Y. H., Gorrie, C. L., Howden, B. P. & Carter, G. P. Genomic Insights
1089 Into Last-Line Antimicrobial Resistance in Multidrug-Resistant *Staphylococcus* and
1090 Vancomycin-Resistant *Enterococcus*. *Front. Microbiol.* **12**, (2021).
1091 16. Li, L. *et al.* Daptomycin Resistance Occurs Predominantly in vanA-Type Vancomycin-
1092 Resistant *Enterococcus faecium* in Australasia and Is Associated With Heterogeneous
1093 and Novel Mutations. *Front. Microbiol.* **12**, 749935 (2021).
1094 17. Bass, N. M. *et al.* Rifaximin Treatment in Hepatic Encephalopathy. *N. Engl. J. Med.* **362**,
1095 1071–1081 (2010).
1096 18. Shayto, R. H., Abou Mrad, R. & Sharara, A. I. Use of rifaximin in gastrointestinal and liver
1097 diseases. *World J. Gastroenterol.* **22**, 6638–6651 (2016).

1098 19. Sherry, N. L. *et al.* Pilot study of a combined genomic and epidemiologic surveillance
1099 program for hospital-acquired multidrug-resistant pathogens across multiple hospital
1100 networks in Australia. *Infect. Control Hosp. Epidemiol.* **42**, 573–581 (2021).
1101 20. Gorrie, C. L. *et al.* Key parameters for genomics-based real-time detection and tracking
1102 of multidrug-resistant bacteria: a systematic analysis. *Lancet Microbe* **2**, e575–e583
1103 (2021).
1104 21. Miller, W. R., Bayer, A. S. & Arias, C. A. Mechanism of Action and Resistance to
1105 Daptomycin in *Staphylococcus aureus* and Enterococci. *Cold Spring Harb. Perspect. Med.*
1106 **6**, a026997 (2016).
1107 22. Merker, M. *et al.* Transcontinental spread and evolution of *Mycobacterium tuberculosis*
1108 W148 European/Russian clade toward extensively drug resistant tuberculosis. *Nat.*
1109 *Commun.* **13**, 5105 (2022).
1110 23. Brandis, G., Wrande, M., Liljas, L. & Hughes, D. Fitness-compensatory mutations in
1111 rifampicin-resistant RNA polymerase. *Mol. Microbiol.* **85**, 142–151 (2012).
1112 24. Goldstein, B. P. Resistance to rifampicin: a review. *J. Antibiot. (Tokyo)* **67**, 625–630
1113 (2014).
1114 25. Rios, R. *et al.* Genomic Epidemiology of Vancomycin-Resistant *Enterococcus faecium*
1115 (VREfm) in Latin America: Revisiting The Global VRE Population Structure. *Sci. Rep.* **10**,
1116 5636 (2020).
1117 26. Duchêne, S. *et al.* Genome-scale rates of evolutionary change in bacteria. *Microb.*
1118 *Genomics* **2**, e000094 (2016).
1119 27. Lebreton, F. *et al.* Emergence of Epidemic Multidrug-Resistant *Enterococcus faecium*
1120 from Animal and Commensal Strains. *mBio* **4**, e00534-13.

1121 28. Raven, K. E. *et al.* A decade of genomic history for healthcare-associated *Enterococcus*
1122 *faecium* in the United Kingdom and Ireland. *Genome Res.* **26**, 1388–1396 (2016).
1123 29. Sensi, P. History of the Development of Rifampin. *Rev. Infect. Dis.* **5**, S402–S406 (1983).
1124 30. Goel, A., Rahim, U., Nguyen, L. H., Stave, C. & Nguyen, M. H. Systematic review with
1125 meta-analysis: rifaximin for the prophylaxis of spontaneous bacterial peritonitis.
1126 *Aliment. Pharmacol. Ther.* **46**, 1029–1036 (2017).
1127 31. Lee, R. A. *et al.* Daptomycin-Resistant *Enterococcus* Bacteremia Is Associated With Prior
1128 Daptomycin Use and Increased Mortality After Liver Transplantation. *Open Forum Infect.*
1129 *Dis.* **9**, ofab659 (2022).
1130 32. Lee, R. S. *et al.* The changing landscape of vancomycin-resistant *Enterococcus faecium* in
1131 Australia: a population-level genomic study. *J. Antimicrob. Chemother.* **73**, 3268–3278
1132 (2018).
1133 33. Weber, D. *et al.* Rifaximin preserves intestinal microbiota balance in patients undergoing
1134 allogeneic stem cell transplantation. *Bone Marrow Transplant.* **51**, 1087–1092 (2016).
1135 34. Taur, Y. *et al.* Intestinal Domination and the Risk of Bacteremia in Patients Undergoing
1136 Allogeneic Hematopoietic Stem Cell Transplantation. *Clin. Infect. Dis.* **55**, 905–914
1137 (2012).
1138 35. Morley, V. J. *et al.* An adjunctive therapy administered with an antibiotic prevents
1139 enrichment of antibiotic-resistant clones of a colonizing opportunistic pathogen. *eLife* **9**,
1140 e58147 (2020).
1141 36. Lin, W. *et al.* Structural Basis of *Mycobacterium tuberculosis* Transcription and
1142 Transcription Inhibition. *Mol. Cell* **66**, 169-179.e8 (2017).

1143 37. Portelli, S., Phelan, J. E., Ascher, D. B., Clark, T. G. & Furnham, N. Understanding
1144 molecular consequences of putative drug resistant mutations in *Mycobacterium*
1145 *tuberculosis*. *Sci. Rep.* **8**, 15356 (2018).
1146 38. Bender, J. K. *et al.* Update on prevalence and mechanisms of resistance to linezolid,
1147 tigecycline and daptomycin in enterococci in Europe: Towards a common nomenclature.
1148 *Drug Resist. Updat.* **40**, 25–39 (2018).
1149 39. Tran, T. T. *et al.* Whole-Genome Analysis of a Daptomycin-Susceptible *Enterococcus*
1150 *faecium* Strain and Its Daptomycin-Resistant Variant Arising during Therapy. *Antimicrob.*
1151 *Agents Chemother.* **57**, 261–268 (2013).
1152 40. Guérillot, R. *et al.* Convergent Evolution Driven by Rifampin Exacerbates the Global
1153 Burden of Drug-Resistant *Staphylococcus aureus*. *mSphere* **3**, e00550-17.
1154 41. Bæk, K. T. *et al.* Stepwise Decrease in Daptomycin Susceptibility in Clinical
1155 *Staphylococcus aureus* Isolates Associated with an Initial Mutation in *rpoB* and a
1156 Compensatory Inactivation of the *clpX* Gene. *Antimicrob. Agents Chemother.* (2015).
1157 42. Cui, L. *et al.* An RpoB Mutation Confers Dual Heteroresistance to Daptomycin and
1158 Vancomycin in *Staphylococcus aureus*. *Antimicrob. Agents Chemother.* (2010)
1159 doi:10.1128/AAC.00437-10.
1160 43. Snyder, E. E. *et al.* PATRIC: The VBI PathoSystems Resource Integration Center. *Nucleic*
1161 *Acids Res.* **35**, D401–D406 (2007).
1162 44. Wood, D. E., Lu, J. & Langmead, B. Improved metagenomic analysis with Kraken 2.
1163 *Genome Biol.* **20**, 257 (2019).
1164 45. Humphries, R. M. The New, New Daptomycin Breakpoint for *Enterococcus* spp. *J. Clin.*
1165 *Microbiol.* **57**, e00600-19.

1166 46. Lam, M. M. *et al.* Comparative analysis of the complete genome of an epidemic hospital
1167 sequence type 203 clone of vancomycin-resistant *Enterococcus faecium*. *BMC Genomics*
1168 **14**, 595 (2013).
1169 47. Bankevich, A. *et al.* SPAdes: A New Genome Assembly Algorithm and Its Applications to
1170 Single-Cell Sequencing. *J. Comput. Biol.* **19**, 455–477 (2012).
1171 48. Homan, W. L. *et al.* Multilocus sequence typing scheme for *Enterococcus faecium*. *J. Clin.*
1172 *Microbiol.* **40**, 1963–1971 (2002).
1173 49. Minh, B. Q. *et al.* IQ-TREE 2: New Models and Efficient Methods for Phylogenetic
1174 Inference in the Genomic Era. *Mol. Biol. Evol.* **37**, 1530–1534 (2020).
1175 50. Schliep, K. P. phangorn: phylogenetic analysis in R. *Bioinformatics* **27**, 592–593 (2011).
1176 51. Paradis, E. & Schliep, K. ape 5.0: an environment for modern phylogenetics and
1177 evolutionary analyses in R. *Bioinformatics* **35**, 526–528 (2019).
1178 52. Yu, G., Smith, D. K., Zhu, H., Guan, Y. & Lam, T. T.-Y. ggtree: an r package for visualization
1179 and annotation of phylogenetic trees with their covariates and other associated data.
1180 *Methods Ecol. Evol.* **8**, 28–36 (2017).
1181 53. Sherry, N. L. *et al.* An ISO-certified genomics workflow for identification and surveillance
1182 of antimicrobial resistance. *Nat. Commun.* **14**, 60 (2023).
1183 54. Crispell, J., Balaz, D. & Gordon, S. V. HomoplasyFinder: a simple tool to identify
1184 homoplasies on a phylogeny. *Microb. Genomics* **5**, e000245 (2019).
1185 55. Lees, J. A., Galardini, M., Bentley, S. D., Weiser, J. N. & Corander, J. pyseer: a
1186 comprehensive tool for microbial pangenome-wide association studies. *Bioinformatics*
1187 **34**, 4310–4312 (2018).
1188 56. de Been, M. *et al.* Core Genome Multilocus Sequence Typing Scheme for High-
1189 Resolution Typing of *Enterococcus faecium*. *J. Clin. Microbiol.* **53**, 3788–3797 (2015).

1190 57. Silva, M. *et al.* chewBBACA: A complete suite for gene-by-gene schema creation and
1191 strain identification. *Microb. Genomics* **4**, e000166 (2018).
1192 58. Croucher, N. J. *et al.* Rapid phylogenetic analysis of large samples of recombinant
1193 bacterial whole genome sequences using Gubbins. *Nucleic Acids Res.* **43**, e15 (2015).
1194 59. Nguyen, L.-T., Schmidt, H. A., von Haeseler, A. & Minh, B. Q. IQ-TREE: A Fast and
1195 Effective Stochastic Algorithm for Estimating Maximum-Likelihood Phylogenies. *Mol.*
1196 *Biol. Evol.* **32**, 268–274 (2015).
1197 60. Rambaut, A., Lam, T. T., Max Carvalho, L. & Pybus, O. G. Exploring the temporal
1198 structure of heterochronous sequences using TempEst (formerly Path-O-Gen). *Virus*
1199 *Evol.* **2**, vew007 (2016).
1200 61. Suchard, M. A. *et al.* Bayesian phylogenetic and phylodynamic data integration using
1201 BEAST 1.10. *Virus Evol.* **4**, vey016 (2018).
1202 62. Minin, V. N. & Suchard, M. A. Counting labeled transitions in continuous-time Markov
1203 models of evolution. *J. Math. Biol.* **56**, 391–412 (2008).
1204 63. Minin, V. N. & Suchard, M. A. Fast, accurate and simulation-free stochastic mapping.
1205 *Philos. Trans. R. Soc. B Biol. Sci.* **363**, 3985–3995 (2008).
1206 64. Monk, I. R., Tree, J. J., Howden, B. P., Stinear, T. P. & Foster, T. J. Complete Bypass of
1207 Restriction Systems for Major *Staphylococcus aureus* Lineages. *mBio* **6**, e00308-15.
1208 65. Zhang, Y., Werling, U. & Edelmann, W. Seamless Ligation Cloning Extract (SLiCE) Cloning
1209 Method. in *DNA Cloning and Assembly Methods* (eds. Valla, S. & Lale, R.) 235–244
1210 (Humana Press, Totowa, NJ, 2014). doi:10.1007/978-1-62703-764-8_16.
1211 66. Pidot, S. J. *et al.* Increasing tolerance of hospital *Enterococcus faecium* to handwash
1212 alcohols. *Sci. Transl. Med.* **10**, eaar6115 (2018).

1213 67. Nair, A. B. & Jacob, S. A simple practice guide for dose conversion between animals and
1214 human. *J. Basic Clin. Pharm.* **7**, 27–31 (2016).
1215 68. Heine, H. S., Bassett, J., Miller, L., Purcell, B. K. & Byrne, W. R. Efficacy of Daptomycin
1216 against *Bacillus anthracis* in a Murine Model of Anthrax Spore Inhalation. *Antimicrob.*
1217 *Agents Chemother.* **54**, 4471–4473 (2010).
1218 69. Higgs, C. *et al.* Optimising genomic approaches for identifying vancomycin-resistant
1219 *Enterococcus faecium* transmission in healthcare settings. *Nat. Commun.* **13**, 509 (2022).
1220 70. Maechler, F. *et al.* Split k-mer analysis compared to cgMLST and SNP-based core genome
1221 analysis for detecting transmission of vancomycin-resistant enterococci: results from
1222 routine outbreak analyses across different hospitals and hospitals networks in Berlin,
1223 Germany. *Microb. Genomics* **9**, 000937 (2023).
1224 71. Liese, J. *et al.* Expansion of Vancomycin-Resistant *Enterococcus faecium* in an Academic
1225 Tertiary Hospital in Southwest Germany: a Large-Scale Whole-Genome-Based Outbreak
1226 Investigation. *Antimicrob. Agents Chemother.* **63**, e01978-18 (2019).
1227 72. Kralj, T. *et al.* Multi-Omic Analysis to Characterize Metabolic Adaptation of the *E. coli*
1228 Lipidome in Response to Environmental Stress. *Metabolites* **12**, (2022).
1229 73. Liebisch, G. *et al.* Update on LIPID MAPS classification, nomenclature, and shorthand
1230 notation for MS-derived lipid structures. *J. Lipid Res.* **61**, 1539–1555 (2020).
1231 74. Langmead, B. & Salzberg, S. L. Fast gapped-read alignment with Bowtie 2. *Nat. Methods*
1232 **9**, 357–359 (2012).
1233 75. Anders, S., Pyl, P. T. & Huber, W. HTSeq—a Python framework to work with high-
1234 throughput sequencing data. *Bioinformatics* **31**, 166–169 (2015).

1235 76. Rappsilber, J., Ishihama, Y. & Mann, M. Stop and Go Extraction Tips for Matrix-Assisted
1236 Laser Desorption/Ionization, Nanoelectrospray, and LC/MS Sample Pretreatment in
1237 Proteomics. *Anal. Chem.* **75**, 663–670 (2003).
1238 77. Rappsilber, J., Mann, M. & Ishihama, Y. Protocol for micro-purification, enrichment, pre-
1239 fractionation and storage of peptides for proteomics using StageTips. *Nat. Protoc.* **2**,
1240 1896–1906 (2007).
1241 78. Cox, J. & Mann, M. MaxQuant enables high peptide identification rates, individualized
1242 p.p.b.-range mass accuracies and proteome-wide protein quantification. *Nat.*
1243 *Biotechnol.* **26**, 1367–1372 (2008).
1244 79. Rozewicki, J., Li, S., Amada, K. M., Standley, D. M. & Katoh, K. MAFFT-DASH: integrated
1245 protein sequence and structural alignment. *Nucleic Acids Res.* **47**, W5–W10 (2019).
1246 80. Magis, C. *et al.* T-Coffee: Tree-based consistency objective function for alignment
1247 evaluation. *Methods Mol. Biol. Clifton NJ* **1079**, 117–129 (2014).
1248 81. Higgins, D. G. & Sharp, P. M. CLUSTAL: a package for performing multiple sequence
1249 alignment on a microcomputer. *Gene* **73**, 237–244 (1988).
1250 82. Rodrigues, C. H. M., Pires, D. E. V. & Ascher, D. B. DynaMut2: Assessing changes in
1251 stability and flexibility upon single and multiple point missense mutations. *Protein Sci.*
1252 *Publ. Protein Soc.* **30**, 60–69 (2021).
1253 83. Nguyen, T. B., Myung, Y., de Sá, A. G. C., Pires, D. E. V. & Ascher, D. B. mmCSM-NA:
1254 accurately predicting effects of single and multiple mutations on protein-nucleic acid
1255 binding affinity. *NAR Genomics Bioinforma.* **3**, lqab109 (2021).
1256 84. Pader, V. *et al. Staphylococcus aureus* inactivates daptomycin by releasing membrane
1257 phospholipids. *Nat. Microbiol.* **2**, 1–8 (2016).

1258 85. Perez-Riverol, Y. *et al.* The PRIDE database resources in 2022: a hub for mass
1259 spectrometry-based proteomics evidences. *Nucleic Acids Res.* **50**, D543–D552 (2022).
1260

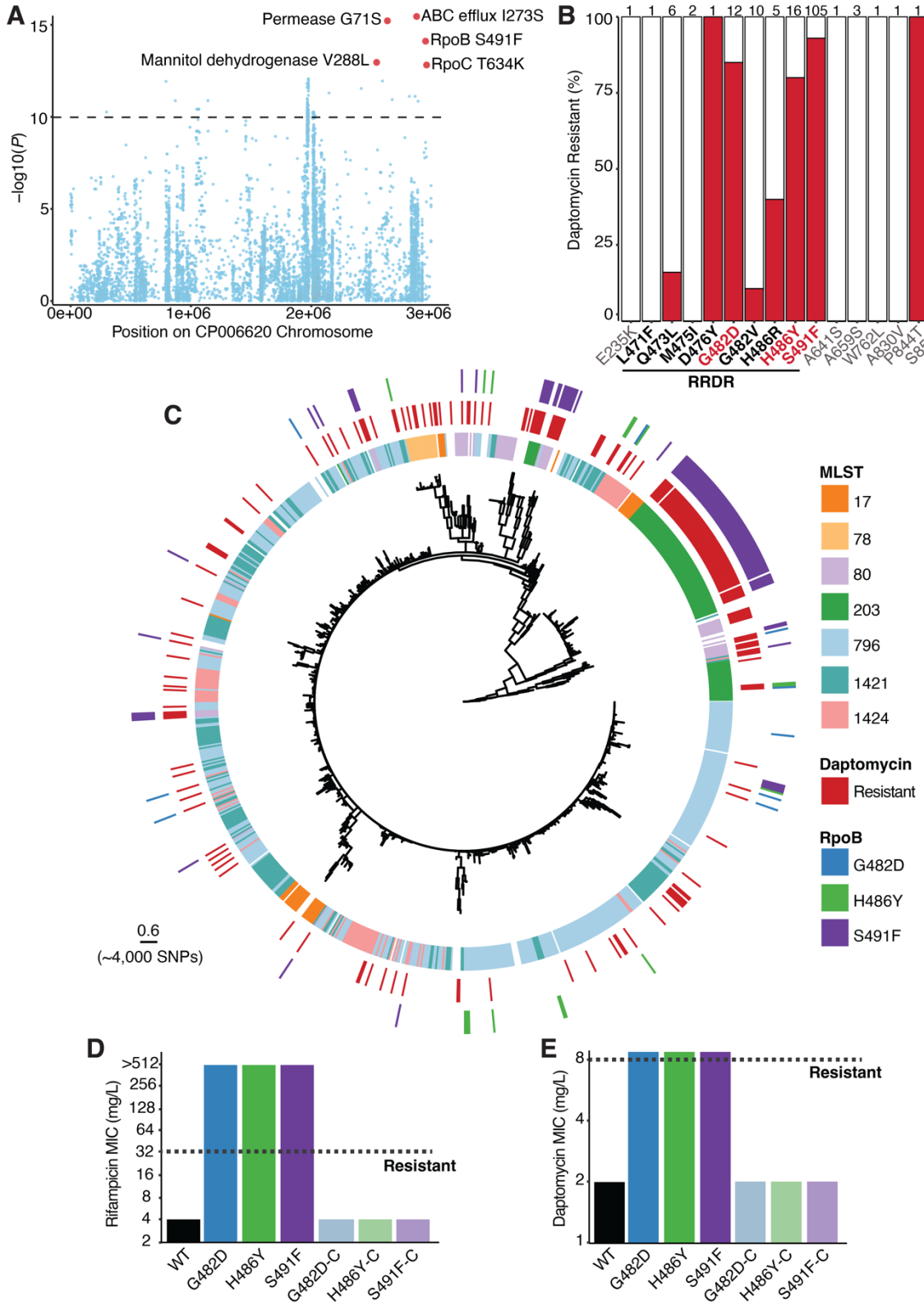
A
Permease G71S
ABC efflux I273S
RpoB S491F
RpoC T634K
Mannitol dehydrogenase V288L
−log10(P)
Position on CP006620 Chromosome
B
Daptomycin Resistant (%)
E235K
L471F
Q473L
M475I
D476Y
G482D
G482V
H486R
H486Y
S491F
A641S
A659S
W762L
A830V
P844T
S851F
P959H
N1196S
RRDR
C
MLST
17
78
80
203
796
1421
1424
Daptomycin
Resistant
RpoB
G482D
H486Y
S491F
0.6
(~4,000 SNPs)
D
Rifampicin MIC (mg/L)
Resistant
WT
G482D
H486Y
S491F
G482D-C
H486Y-C
S491F-C
E
Daptomycin MIC (mg/L)
Resistant

1261

1262 **Figure 1. A.** Manhattan plot of 10,530 variants, displayed by position on the reference genome
1263 and significance association with daptomycin resistance (univariate analysis using a linear
1264 mixed model). The dashed line shows the Bonferroni-corrected significance threshold. **B.**
1265 Percentage of daptomycin-resistant strains for each mutation within RpoB. The mutations
1266 within the rifampicin resistance determining region (RRDR) are shown in bold. Mutations
1267 coloured in red were associated with daptomycin resistance. The total number of strains
1268 containing each mutation is shown above each bar. **C.** Maximum-likelihood core-SNP-based
1269 phylogeny of clinical VREfm (n=1000) inferred from 6,574 SNPs, demonstrating the presence
1270 of RpoB mutations in daptomycin-resistant isolates. Overlaid are the results of *in silico* multi-
1271 locus sequence type (MLST), daptomycin phenotypic testing, and mutations associated with
1272 daptomycin resistance in RpoB. In the first circle, ST is not shown for uncommon STs ($n \leq 5$).
1273 The scale bar indicates number of nucleotide substitutions per site (top), with an
1274 approximation of SNP distance (in parentheses). **D.** Rifampicin susceptibility testing results for
1275 the WT and isogenic *rpoB* mutants and complement strains (designated with -C) (n=3). **E.**
1276 Daptomycin susceptibility testing results for the WT and isogenic *rpoB* mutants and
1277 complemented strains (designated with -C) (n=3). The MIC for each strain is shown without
1278 error bars since there was no variation between the independent biological replicates.

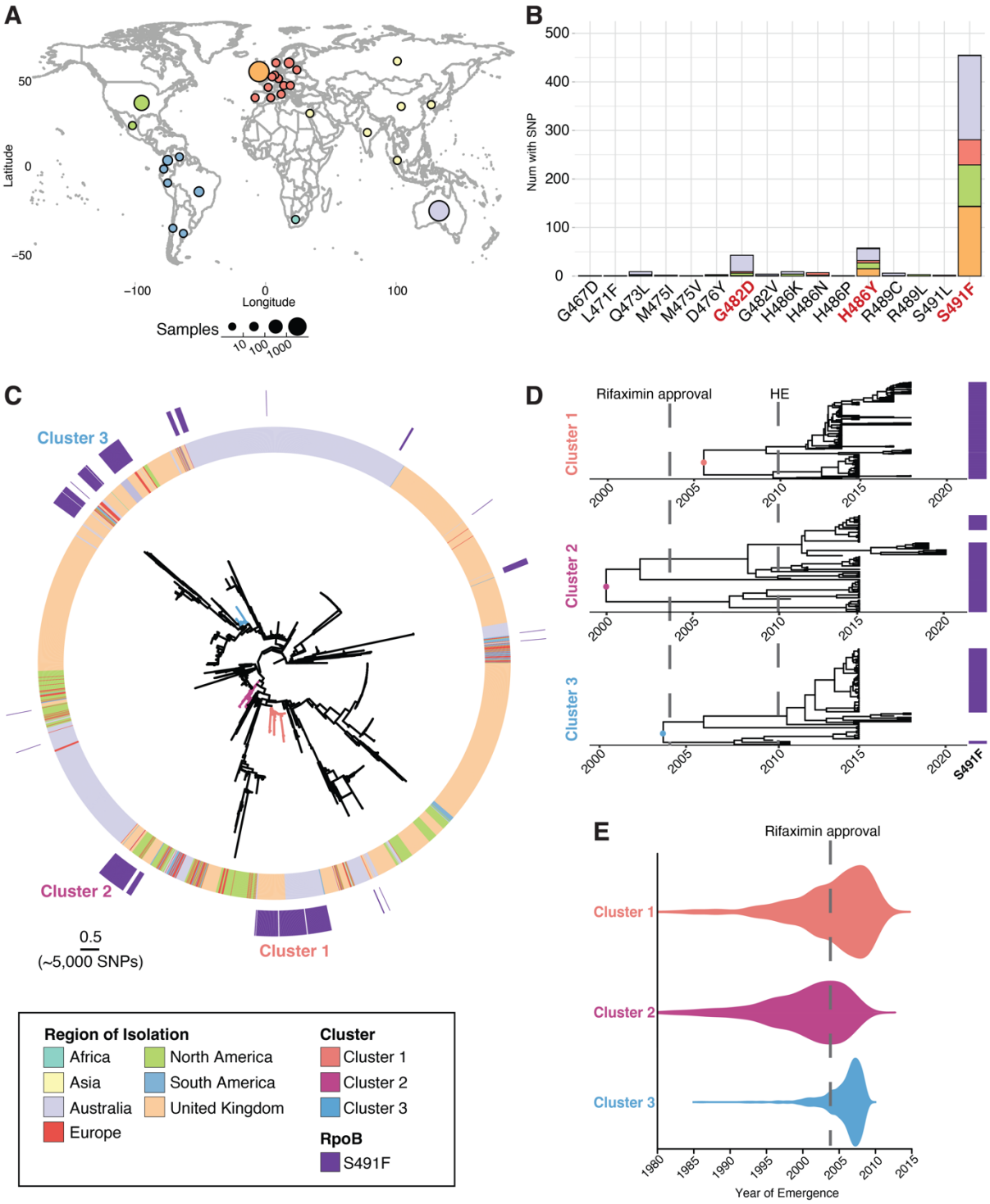
A
Latitude
50
0
−50
−100
0
100
Longitude
Samples
10
100
1000
B
Num with SNP
500
400
300
200
100
0
G467D
L471F
Q473L
M475I
M475V
D476Y
G482D
G482V
H486K
H486N
H486P
H486Y
R489C
R489L
S491L
S491F
C
Cluster 3
Cluster 2
Cluster 1
0.5
(~5,000 SNPs)
D
Rifaximin approval
HE
Cluster 1
Cluster 2
Cluster 3
2000
2005
2010
2015
2020
S491F
E
Rifaximin approval
Cluster 1
Cluster 2
Cluster 3
1980
1985
1990
1995
2000
2005
2010
2015
Year of Emergence
Region of Isolation
Africa
Asia
Australia
Europe
North America
South America
United Kingdom
Cluster
Cluster 1
Cluster 2
Cluster 3
RpoB
S491F

1279

1280 **Figure 2. A.** Map of 4,476 VREfm genomes included in this study. Circle size corresponds to
1281 total number of genomes (binned into categories), and colour corresponds to region of
1282 isolation. Country coordinates used are the country centroid position. **B.** The frequency of
1283 various RpoB mutations within the rifampicin resistance determining region (RRDR) in 4,476
1284 VREfm genomes, sampled from 43 MLSTs. Bars are coloured by the number of isolates from
1285 each region of isolation containing the mutation. The identified daptomycin resistance
1286 associated mutations are coloured in red. **C.** Maximum-likelihood, core-SNP-based phylogeny
1287 for 4,476 VREfm inferred from 9,277 core-genome SNPs, demonstrating the presence of the
1288 S491F RpoB mutation in international VREfm. Overlaid is the region of isolation for each strain
1289 and the presence of the S491F mutation. The coloured branches indicate the three VREfm
1290 clusters identified with cgMLST used as input for Bayesian evolutionary analyses. The scale
1291 bar indicates number of nucleotide substitutions per site (top), with an approximation of SNP
1292 distance (in parentheses). **D.** Bayesian phylodynamic analyses showing the maximum-clade
1293 credibility (MCC) trees of the three VREfm clusters with the timing of emergence for each
1294 lineage. The median substitution rate was similar for Cluster 1 and Cluster 2, at 9.7x10-7 [95%
1295 highest posterior density (HPD) 6.88x10-7 – 1.24x10-6] and 1.25x10-6 (95% HPD 7.68x10-7 –
1296 1.74x10-6) respectively, but slightly faster for Cluster 3 at 3.86x10-6 (95% HPD 2.23x10-6 –
1297 5.69x10-6). Cluster 1 (n=219) was inferred from a core alignment of 1,869,554 bp containing
1298 329 SNP sites; Cluster 2 (n=85) was inferred from an alignment of 1,524,024 bp containing 541
1299 SNP sites; and Cluster 3 (n=68) was inferred from an alignment of 1,860,780 bp containing 764
1300 SNP sites. The time in years is given on the *x* axis. The presence of the S491F RpoB trait for
1301 each isolate is shown in purple. Overlaid onto the MCC trees is the first instance of FDA
1302 approval for rifaximin (2004) and for hepatic encephalopathy (HE) (2010). **E.** Violin plots for
1303 the most recent common ancestor (MCRA) for each cluster, representing when the RpoB

1304 S491F mutation first emerged, with 95% HPD intervals – 2006 (HPD 1993 – 2012) for Cluster

1305 1, 2000 (HPD 1989 – 2008) for Cluster 2, and 2004 (HPD 2001 – 2010) for Cluster 3. Overlaid

1306 onto violin plots is the FDA approval date for rifaximin (2004).

1307

1308

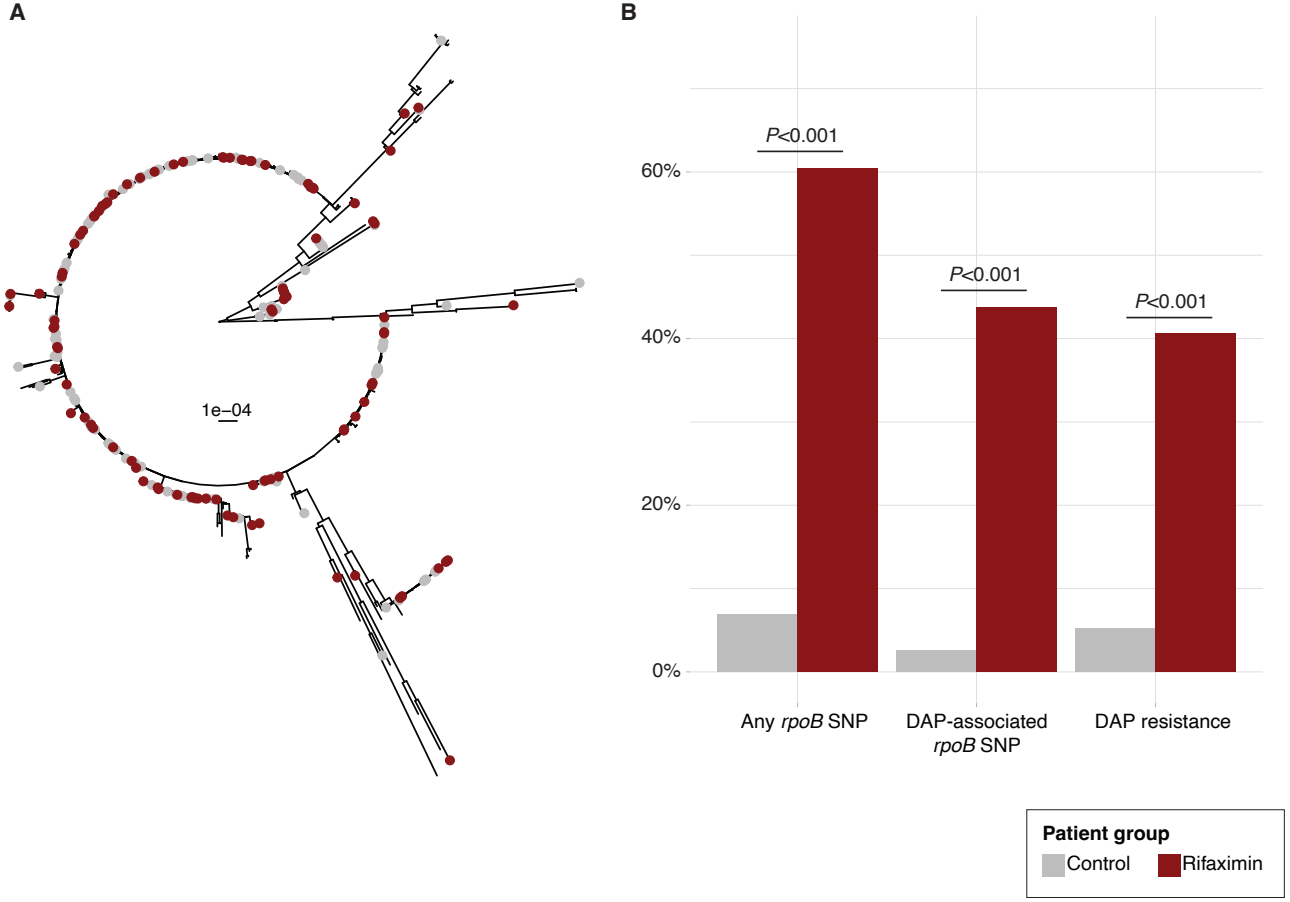

1309

1310

1311 **Figure 3. A.** Maximum-likelihood, core-SNP-based phylogeny for VREfm inferred from 14,420
1312 core-genome SNPs, demonstrating which isolates were from the “control” or “rifaximin”
1313 groups. The scale bar indicates number of nucleotide substitutions per site. **B.** Summary of
1314 the percentage of VREfm with any *rpoB* SNP, daptomycin (DAP)-associated *rpoB* SNP (S491F,
1315 G482D and H486Y), or DAP resistance in patients in the “control” or “rifaximin” groups. Data
1316 was analysed using a Fisher’s exact test.
1317

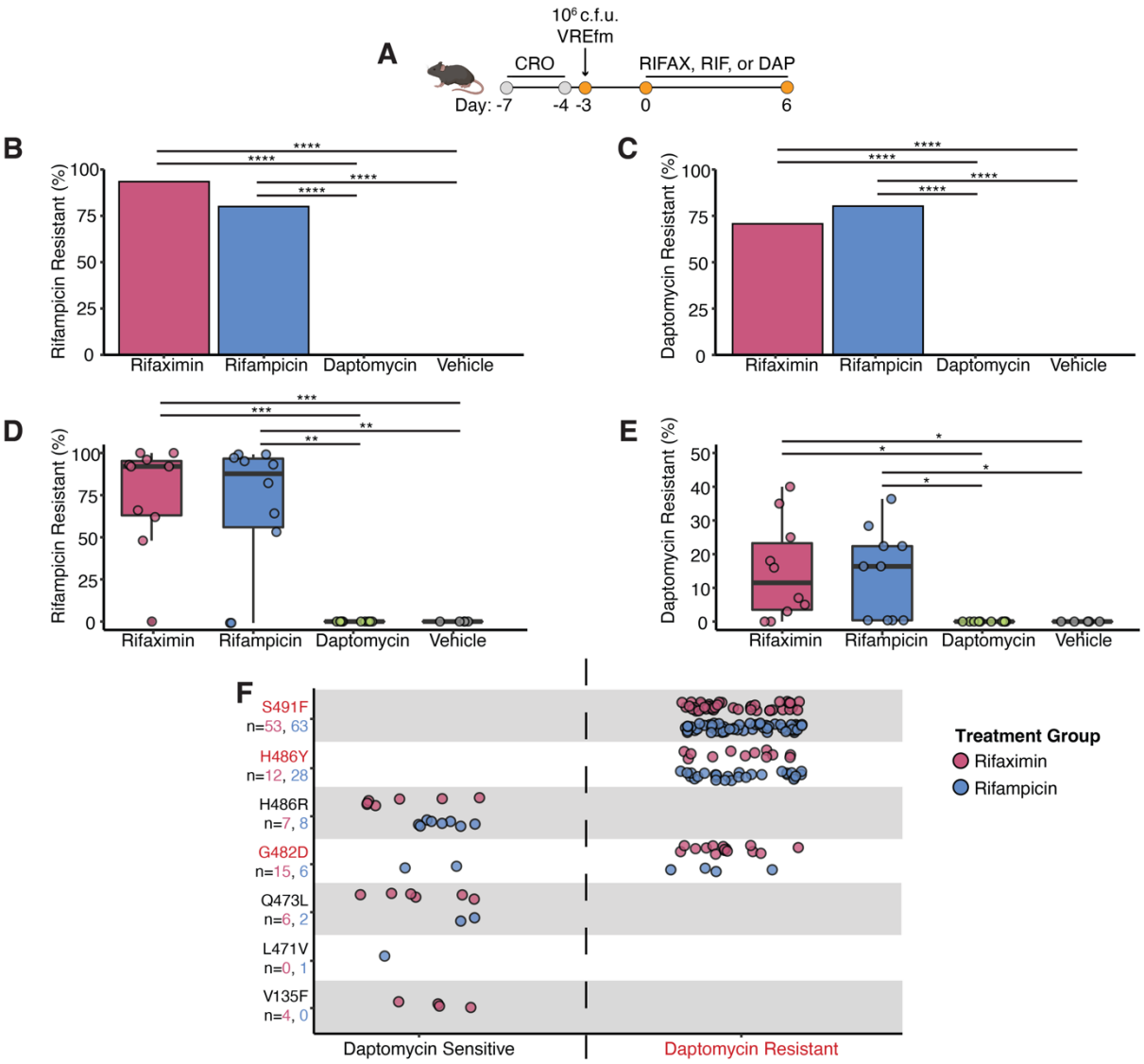
A
10⁶ c.f.u.
VREfm
CRO
RIFAX, RIF, or DAP
Day: -7
-4 -3
0
6
B
Rifampicin Resistant (%)
Rifaximin
Rifampicin
Daptomycin
Vehicle
C
Daptomycin Resistant (%)
D
E
F
S491F
n=53, 63
H486Y
n=12, 28
H486R
n=7, 8
G482D
n=15, 6
Q473L
n=6, 2
L471V
n=0, 1
V135F
n=4, 0
Daptomycin Sensitive
Daptomycin Resistant
Treatment Group
Rifaximin
Rifampicin

1318

1319 **Figure 4. A.** Timeline of the mouse experiment. VREfm-colonised mice (n=5 for vehicle, n=10
1320 for rifampicin, n=10 for rifaximin, n=10 for daptomycin) received a human-equivalent dose of
1321 vehicle, rifampicin, or rifaximin (twice per day for rifaximin) for 7 days by oral gavage or
1322 subcutaneous injection with daptomycin for 7 days. CRO=ceftriaxone; DAP=daptomycin;
1323 RIFAX=rifaximin; RIF=rifampicin. Figure to scale. **B.** Percentage of total mice with rifampicin-
1324 resistant VREfm strains **C.** or daptomycin-resistant VREfm strains after 7 days of antibiotic
1325 treatment. **D.** Percentage of VREfm from each mouse (n=50 colonies per mouse) that were
1326 resistant to rifampicin **E.** or daptomycin after 7 days of antibiotic treatment. Points represent
1327 an individual mouse. Percentage was calculated from rifampicin or daptomycin MIC values
1328 (either resistant or susceptible) from 50 VREfm colonies isolated from each mouse. Boxes
1329 represent the median and interquartile range for each group. **F.** Overview of the RpoB
1330 mutations identified in the rifampicin-resistant colonies. Each point represents a single colony.
1331 Isolates are separated by each RpoB mutation and grouped into either daptomycin-
1332 susceptible or daptomycin-resistant. The RpoB mutations coloured in red had an association
1333 with daptomycin resistance; n values represent the number of isolates containing each
1334 mutation for rifaximin and rifampicin, respectively. *$P < 0.05$, **$P < 0.01$, ***$P < 0.001$,
1335 ****$P<0.0001$; unpaired *t*-test (vehicle versus rifampicin or vehicle versus rifaximin and
1336 rifampicin verses daptomycin or rifaximin verses daptomycin).

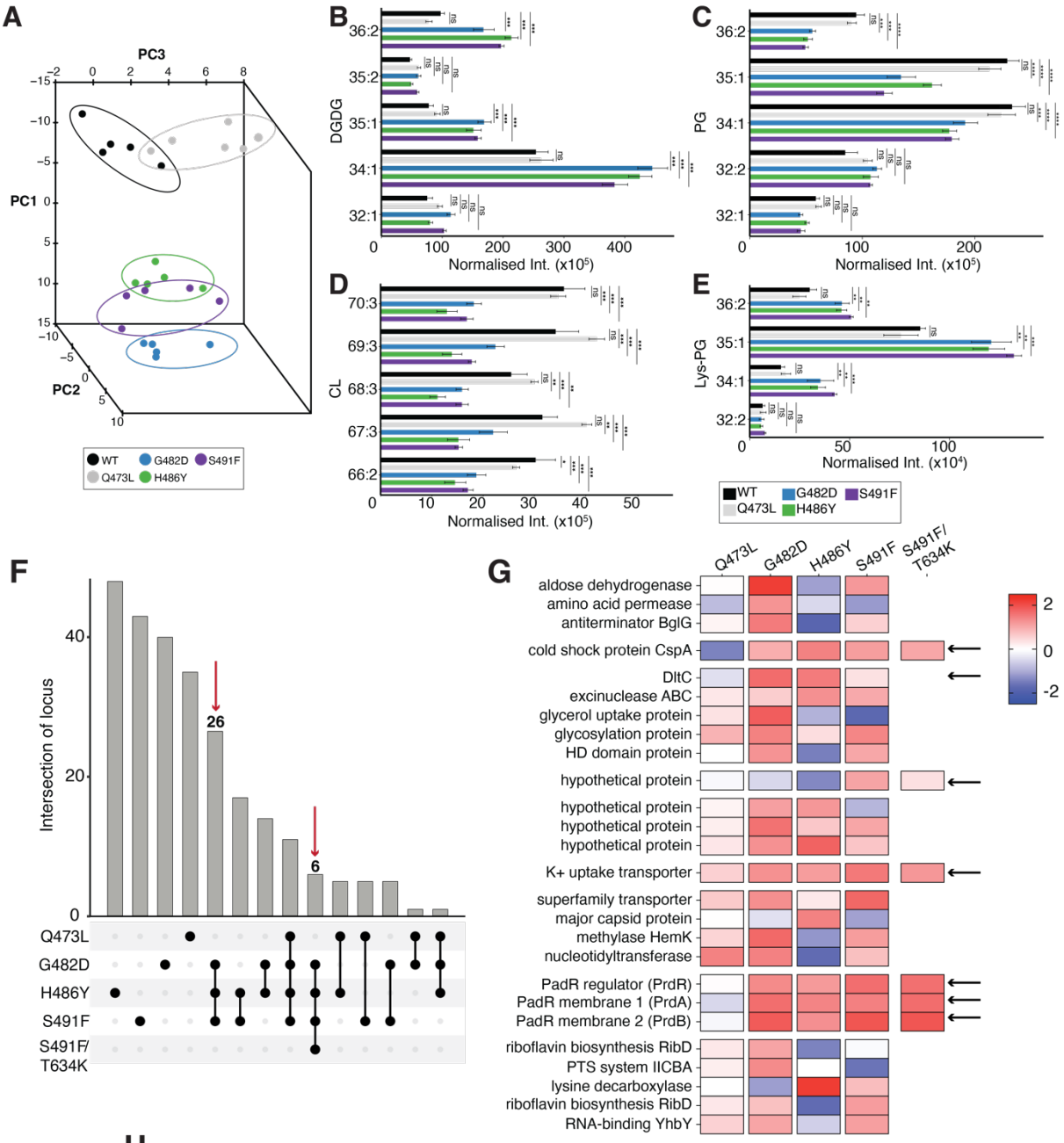
A
PC3
PC1
PC2
WT
G482D
S491F
Q473L
H486Y
B
DGDG
36:2
35:2
35:1
34:1
32:1
Normalised Int. (x10⁵)
C
PG
36:2
35:1
34:1
32:2
32:1
Normalised Int. (x10⁵)
D
CL
70:3
69:3
68:3
67:3
66:2
Normalised Int. (x10⁵)
E
Lys-PG
36:2
35:1
34:1
32:2
Normalised Int. (x10⁴)
F
Intersection of locus
26
6
Q473L
G482D
H486Y
S491F
S491F/
T634K
G
Q473L
G482D
H486Y
S491F
S491F/
T634K
aldose dehydrogenase
amino acid permease
antiterminator BglG
cold shock protein CspA
DltC
excinuclease ABC
glycerol uptake protein
glycosylation protein
HD domain protein
hypothetical protein
hypothetical protein
hypothetical protein
hypothetical protein
K+ uptake transporter
superfamily transporter
major capsid protein
methylase HemK
nucleotidyltransferase
PadR regulator (PrdR)
PadR membrane 1 (PrdA)
PadR membrane 2 (PrdB)
riboflavin biosynthesis RibD
PTS system IICBA
lysine decarboxylase
riboflavin biosynthesis RibD
RNA-binding YhbY
H
WT
S491F
G482D
H486Y
DAP MIC (mg/L)
WT
ΔprdR
ΔprdA
ΔprdB
S491F
S491F ΔprdR
S491F ΔprdA
S491F ΔprdB
G482D
G482D ΔprdR
G482D ΔprdA
G482D ΔprdB
H486Y
H486Y ΔprdR
H486Y ΔprdA
H486Y ΔprdB

1337

1338 **Figure 5. A.** Principal-component analysis denoting segregation of the total lipid classes
1339 obtained for the WT and RpoB mutants. **B to E.** The lipid species differentially produced by the
1340 WT and RpoB mutants are showed as normalised abundance (intensity/total protein). Bars
1341 represent the median value and error bars represent the SEM (n=5). Data was analysed with
1342 a Two-way ANOVA (WT versus RpoB mutant) **F.** Intersection between RNAseq and proteomics
1343 analyses displayed as an UpSet plot (n=5 for RNAseq and n=5 for proteomics). RNA seq
1344 significance (FDR<0.05, $\log_2$FC > 1 or $\log_2$FC < -1) and proteomics significance (adjusted p-
1345 value<0.05, $\log_2$FC > 1 or $\log_2$FC < -1). **G.** Heatmaps displaying the 26 significantly, differentially
1346 expressed loci identified in both RNA seq and proteomics. The fold-change value for RNAseq
1347 is shown. **H.** Daptomycin susceptibility testing results for the WT and *rpoB* backgrounds with
1348 *prdR*, *prdA*, or *prdB* deleted (n=3). The MIC for each strain is shown without error bars since
1349 no variation between independent biological replicate was observed. ns not significant, *P <
1350 0.05, **P < 0.01, ***P < 0.001, ****P<0.0001.
1351

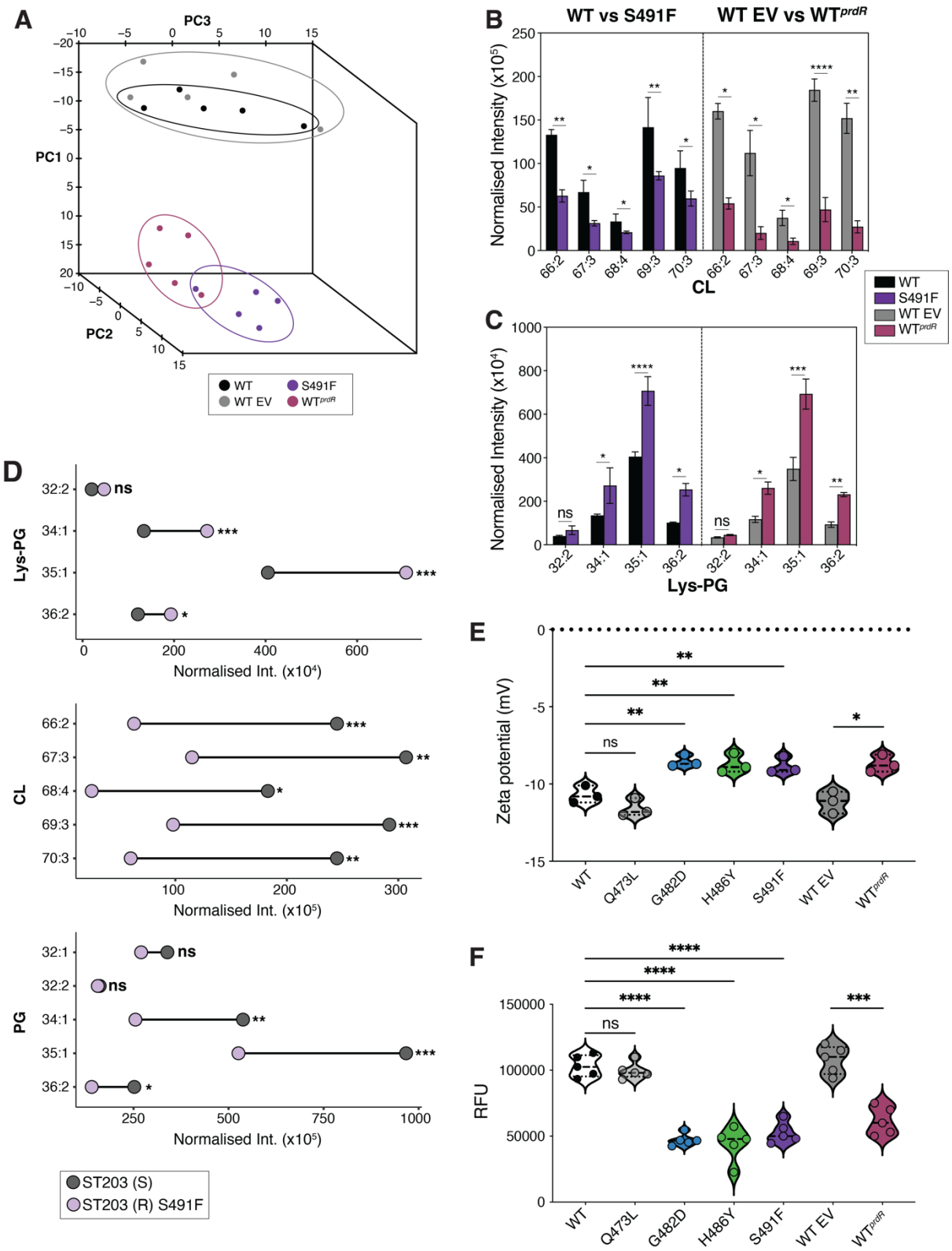
A
PC3
PC1
PC2
WT
S491F
WT EV
WTprdR
B
WT vs S491F
WT EV vs WTprdR
Normalised Intensity (x10⁵)
CL
C
Normalised Intensity (x10⁴)
Lys-PG
D
Lys-PG
Normalised Int. (x10⁴)
CL
Normalised Int. (x10⁵)
PG
Normalised Int. (x10⁵)
ST203 (S)
ST203 (R) S491F
E
Zeta potential (mV)
F
RFU

1352

1353 **Figure 6. A.** Principal-component analysis denoting segregation of the total lipid classes
1354 obtained for the WT, S491F mutant, WT empty vector (EV), and WT^{prdR}. **B and C.** The lipid
1355 species differentially produced by the WT, S491F mutant, WT EV, and WT^{prdR} are showed as
1356 normalised abundance (intensity/total protein). Bars represent the median value and error
1357 bars represent the SEM (n=5). Data was analysed with a Two-way ANOVA (WT versus RpoB
1358 mutant and WT EV versus WT^{prdR}). **D.** Lipid species differentially produced by the ST203 RpoB
1359 S491F clinical strain pair, showed as normalised abundance (intensity/total protein). The dots
1360 represent the median value (n=5). Data was analysed with a Two-way ANOVA (ST203 DAP-S
1361 versus ST203 DAP-R). Lipid species with a significant difference are denoted. **E.** Zeta potential
1362 (measured in mV). Points represent each biological replicate (n=3) and lines represent the
1363 median and interquartile range. Data was analysed with a Two-way ANOVA (WT versus RpoB
1364 mutant and WT EV versus WT^{prdR}). **F.** Binding of BoDIPY-DAP, represented as relative
1365 fluorescence units (RFU). Points represent each biological replicate (n=5) and lines represent
1366 the median and interquartile range. Data was analysed with a Two-way ANOVA (WT versus
1367 RpoB mutant and WT EV versus WT^{prdR}). ns not significant, *$P < 0.05$, **$P < 0.01$, ***$P < 0.001$,
1368 ****$P<0.0001$.

1369
1370